Rebuttal to “Interannual drivers of the seasonal cycle of CO_2 fluxes in the Southern Ocean”

by Gregor, Kok and Monteiro

Overview of changes

The authors would like to thank the reviewers for their recommendations to improve the manuscript. The changes are relatively substantial with the manuscript now being more succinct. The major scientific changes are: 1) removal of the two high resolution methods; 2) inclusion of uncertainty estimates. We also apologise for the multitude of typos and figure reference errors throughout the document. We hope that the reviewers now find the manuscript in a more presentable state.

In the document below we show the initial response of the reviewers in blue and the responses to each point in black. Track changes for the manuscript are shown below the response to the reviewer.

Reviewer 2

Overview

The authors present here a lengthy paper in which they aim to provide evidence that the included machine learning products for pCO2 are an appropriate proxy for investigating interannual variability in pCO2 and carbon fluxes in the Southern Ocean. They use these products to analyse transitions between regimes and also investigate the drivers of the changes. However, the paper needs to be proofread prior to submitting as it has errors throughout which distracts from the science. The job of a review is not to be a technical reviewer but to analyse the science. Unfortunately it is difficult to follow the science with the errors included throughout the paper.

Major revision

The authors utilize an ensemble of five products for this study, however 2 of the products are just a repetition of two other products produced at a higher resolution. There is no evidence given that this results in 5 independent products for this ensemble. At the very least, more discussion is required for it to be accepted that the high and low resolution versions of the same product can be seen as individual ensemble members.

We acknowledge that these two high resolution implementations may not have contributed results that were mechanistically different to the low resolution implementations. We have thus removed the high resolution data from the study. This means that the now reduced ensemble includes only three machine learning methods: SOM-FFN, SVR, RFR.

Additionally, the analysis should be revised to include the SOM-FFN created with SOCATv3 so that all members are produced using the same dataset. The SOM-FFN product is available based on SOCATv4 now and the authors should at least update it to the version based on SOCATv3 (see https://www.nodc.noaa.gov/ocads/oceans/SPCO2_1982_2015_ETH_SOM_FFN.html).

We now use v2.2 of the SOM-FFN implementation which used SOCAT v4. The results have been updated accordingly.

This paper is wrought with inconsistencies, incomplete definitions, and missed words which distracts the reader throughout. Some examples include the use of MIZ in text but AZ in figures, along with a consistent use of acronyms without first defining them (PFZ, AZ, MIZ, etc). Additionally, using the Fay & McKinley biome boundaries but then referring to the regions as SAZ, PFZ, AZ/MIZ is confusing and inaccurate. The biomes and frontal regions are not interchangeable and the authors need to be consistent throughout the study as to which they are using.

These abbreviations based on the Fay and McKinley (2014) paper where the authors state: *"…Southern Ocean regions that we define as STSS, SPSS and ICE biomes. Respectively, these three Southern Ocean biomes are comparable to the Sub-Antarctic Zone (SAZ), the Polar Frontal Zone (PFZ) and Antarctic Zone (AZ)".* We chose to use MIZ instead of AZ. These biomes are now defined before they are used. If the reviewer still feels that these should be changed, we would be happy to make these changes.

In Figure 2, the different extents into the ice covered regions of each product will affect the comparison shown in 2c. Ensure that equal regions are being compared. Also, showing how the products compare to the available data in Figure 2 would be helpful.

We have changed the comparison area to be consistent for all models. This means that a large

portion of the MIZ/ICE is omitted. We have thus decided to exclude the MIZ from the rest of the analysis. We do show the MIZ data for both ΔpCO_2 and FCO_2 in the Supplementary materials. The available data is unfortunately just too sparse to plot alongside the empirical estimates on a monthly scale as shown in the figure below.

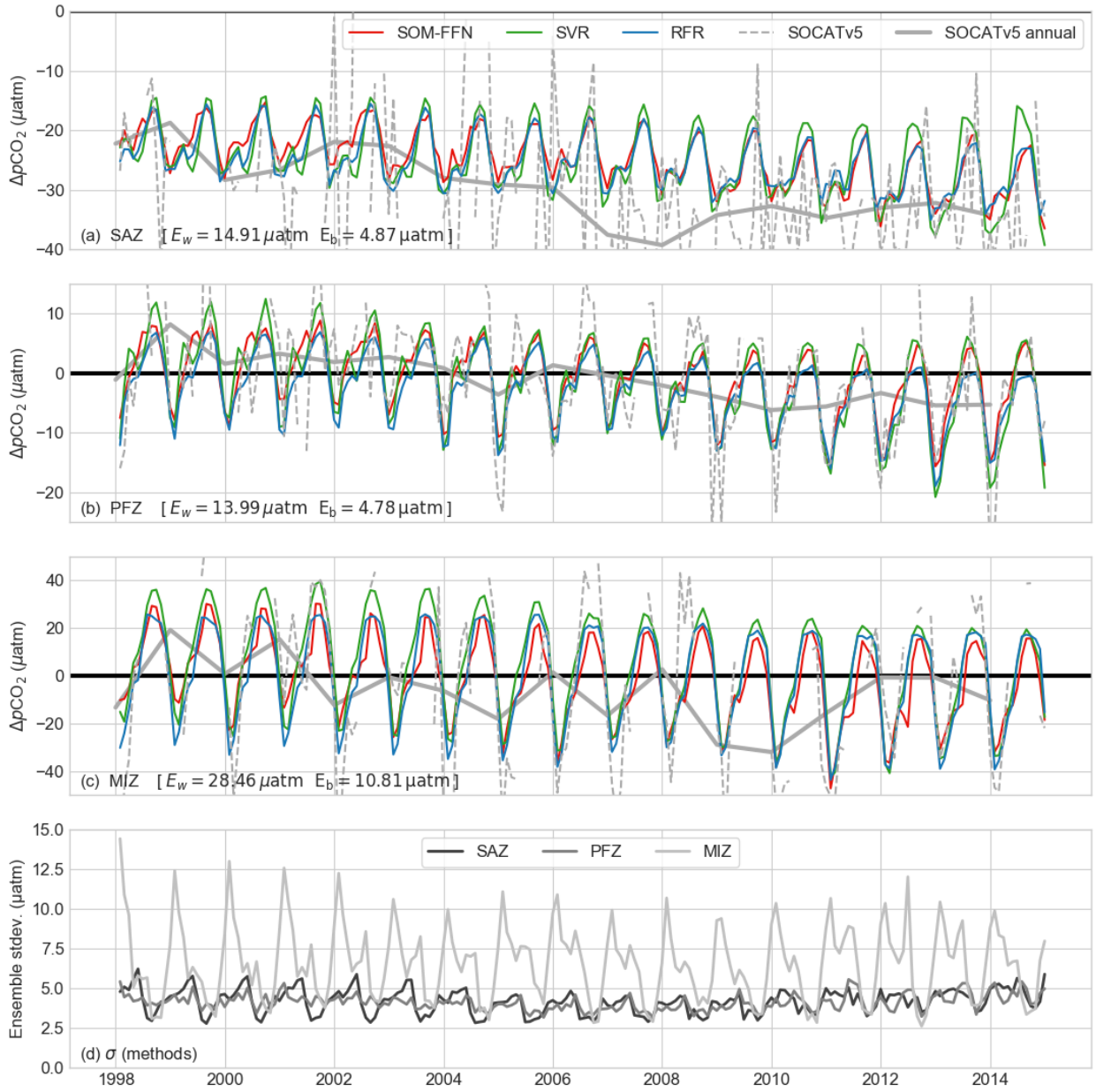

R1: Figure is the same as Figure 2 in the manuscript with the addition of the SOCAT v5 data.

Figure 3b is not discussed in the text at all. The definition of the "signal" as the largest difference in trend for a particular grid cell should be referenced as typically it is the mean trend/value that is the "signal" and the noise is the spread around that signal (either standard deviation, standard error, etc).

Figure 3 has been removed from the manuscript. We now take a different approach in addressing the uncertainties at the request of Reviewer 1.

Figures 5 and 6 need to be improved dramatically. The difference between the dark and light curves in Figure 5 is not defined. Additionally, there is no indication of which product (or average of the ensemble) is being plotted here. The captions are wrong (referenced subplots j-r which do not exist). The background grey shading to designate the difference regimes/timescales is difficult to distinguish. Perhaps another method to highlight those would be helpful. Additionally, trends included on these figures should have confidence intervals or uncertainty values included.

We have changed this figure substantially. The MIZ has been dropped as the small remaining area (after masking for model inconsistency) is not representative of the biome. This has thus simplified the image a lot. We have darkened the shading as we too noticed that these are very light when the manuscript is printed. We have also included the dates of these periods on the figure. Note that the dates of the periods have changed at the request of Reviewer 1. The captions have been corrected.

We have also moved the figure showing the fluxes to the supplementary materials. We feel that this distracts slightly from the story that we are trying to tell. Moreover, we have removed the trends from the Flux figure as it is confusing to work with anomalies and then present trends (Reviewer 1).

Figures 7-8 continue with captions that do not correspond to the figure ("wind stress (d-e), SST (f-h)" when wind stress is in (d-f) and SST in (g-i), etc.

We have corrected these captions.

Technical Corrections

Below are some obvious technical corrections which I have not already addressed above. I reiterate though that the entire paper needs to be revised and improved, as it is difficult to follow the science with incorrect references to figures and missing words in sentences.

- Line 43: "not due to changes in overturning"
  I wasn't completely sure what the reviewer found at fault in this sentence other than being clumsy. It has been rephrased: *"While previous studies suggested that changes in wind strength have led to changes in meridional overturning and thus CO_2 uptake (Lenton and Matear, 2007; Lovenduski et al., 2007; Lenton et al., 2009; DeVries et al., 2017), Landschützer et al. (2015) suggested that atmospheric circulation has become more zonally asymmetric since the mid 2000's, which has led to an oceanic dipole of cooling and warming."*
- Line 46: "The led to an oceanic dipole. . ."
  "...which has led to an oceanic dipole…"
- Line 62: repeated word
  Removed
- Line 141: PFZ and MIZ not defined. MIZ and AZ used inter- changeably throughout paper
  We now define these when first introduced on L165.
- Line 149: missing a word in "the variability of between the ensemble members. . ."
  This has been rephrased to: *"The first section examines the uncertainties of the ensemble and its members."*

- Line 157: how are “scores” calculated?
  We now define the scores explicitly as the root mean squared error (RMSE).
- Line 199: Should reference Figure 3c I believe
  Figure has been removed
- Line 213: Figures 2a-c and 4a-c are not the correct reference figures for the points being addressed.
  The references to figures have (hopefully) been corrected
- Line 221: “CO2”
  We have corrected all occurrences of CO_2 to be subscripted
- Line 255-260: Figure 5 caption is inaccurate to what is shown in Figure 5
  Corrected and figure numbers have changed
- Line 289: Should reference Figure 5a,d rather than Figure 5 b,e.
  Corrected and figure numbers have changed
- Line 291: remain consistent with capitalizing Southern Ocean
  All occurrences of Southern Ocean have now been capitalised
- Line 307: Do you mean the seasonal cycle amplitude?
  We define this at the first occurrence of the phrase on L211
- Line 342: “it was advanced that the explanation. . .” is awkward
  This section has changed a great deal – this paragraph has been removed
- Line 350: “These studies have in linked the wind stress variability. . .” is awkward and needs to be rewritten.
  This has been removed
- Lines 373-376: caption for Figure 7 and Figure 8 need to be corrected to accurately reference the figures.
  The captions have been corrected
- Line 387-388: “. . .and surrounds (Figure 7d,j)” is awkward. Consider revising sentence
  Rephrased to: *This regional sustained saturation corresponds to a shift towards stronger winds and/or deeper MLDs in the west Pacific sector of the SAZ (Figure 5d,j).*
- Line 397: “(-ve shift)”. Is this supposed to be negative shift? If so, simply spell out to improve clarity.
  All occurrences of +ve and –ve have been written out as positive and negative respectively.
- Line 439: “ENSE” perhaps should be ENSO?
  Changed to ENSO

Overall, the science presented in the paper is interesting and could provide a interested look at using various machine learning methods to gain an understanding of the Southern Ocean carbon drivers. However, the lack of proofreading prior to submitting is clear and must be improved before a complete review of the manuscript can be undertaken.

Interannual drivers of the seasonal cycle of CO_2 ~~fluxes~~ in the Southern Ocean

Luke Gregor[1,2], Schalk Kok[3] and Pedro M. S. Monteiro[1]

[1] Southern Ocean Carbon-Climate Observatory (SOCCO), CSIR, Cape Town, South Africa
[2] University of Cape Town, Department of Oceanography, Cape Town, South Africa
[3] University of Pretoria, Department of Mechanical and Aeronautical Engineering, Pretoria, South Africa

Correspondence to: Luke Gregor ~~(luke.gregor@uct.ac.za)~~(luke.gregor@uct.ac.za)

Abstract. Machine learning ~~methods (support vector regression and random forest regression) were used~~has become a useful tool to ~~map gridded estimates~~interpolate ship measurements of ~~Δ~~pCO_2 ~~in the Southern Ocean from (~~SOCAT ~~v3)~~ to a gridded map using satellite data. ~~A low (1° × monthly) and high (0.25° × 16-day) resolution implementation of each of these methods as well as~~ In this study we use an ensemble of three machine learning methods: Support Vector Regression (SVR) and Random Forest Regression (RFR) from Gregor et al. (2017); and the SOM-FFN method ~~of~~from Landschützer et al. ~~(2014) were added to a five member ensemble.~~(2016). The ~~ensemble mean ΔpCO_2 was used to calculate FCO_2 (air-sea CO_2 flux). Data was~~ interpolated data were separated into nine ~~domains~~regions defined by basin (Indian, Pacific and Atlantic) and biomes (as defined by Fay and McKinley ~~(2014~~, 2014a). The regional approach showed ~~large~~ a meridional gradient and zonal asymmetry in the magnitude of ΔpCO_2 ~~and FCO_2~~ estimates. Importantly, there was a seasonal decoupling of the modes for summer and winter interannual variability. Winter ~~trends~~ interannual variability had a ~~larger 10 year~~longer mode of variability compared to summer ~~trends~~, which ~~had~~varied on a ~~shorter~~ 4–6 year ~~mode~~time scale. To understand this variability of ~~FCO_2~~ΔpCO_2, we ~~separately assessed~~investigated changes in summer and winter ΔpCO_2 and the drivers thereof. The dominant winter changes ~~were~~are driven by wind stress variability. ~~Summer variability correlated well~~This is consistent with the temporal and spatial characteristics of the Southern Annular Mode (SAM), which has a decadal mode of variability (Lovenduski et al., 2008; Landschützer et al., 2016). Interannual trends in summer variability of pCO_2 are consistent with chlorophyll-*a* variability where the latter had high mean seasonal concentrations. In regions of low chlorophyll-*a* concentrations, wind stress and sea surface temperature ~~were lower order~~emerged as stronger drivers of ΔpCO_2. In summary we propose that sub-decadal variability is explained by summer drivers, while winter variability contributes to the long term changes associated with the SAM.

1 Introduction

The Southern Ocean plays a key role in the uptake of anthropogenic CO_2 (Khatiwala et al., 2013; DeVries et al., 2017). Moreover, it has been shown that the Southern Ocean is sensitive to anthropogenically influenced climate variability, such as the intensification of the westerlies (Le Quéré et al., 2007; Lenton et al., 2009; Swart and Fyfe, 2012; DeVries et al., 2017). Until recently, the research community has not been able to accurately measure the contemporary changes, let alone understand the drivers, of CO_2 in the ~~contemporary~~ Southern Ocean due to a paucity of observations (Landschützer et al., 2015). Empirical models provide an interim solution to this challenge until prognostic ocean biogeochemical models are able to represent the Southern Ocean CO_2 seasonal cycle accurately (Lenton et al., 2013; Rödenbeck et al., 2015; Mongwe et al., 2016). ~~There is an agreement in the~~The research community agrees on large changes in CO_2 fluxes in the Southern Ocean from a source in the 1990's to a sink in the 2000's; however, there is disagreement in the drivers of the changes in CO_2 uptake (Lovenduski et al., 2008; Landschützer et al., 2015; DeVries et al., 2017). This study aims to understand the drivers of the changing CO_2 sink in the Southern Ocean based on an ensemble of empirical estimates ~~with~~using a seasonal analysis framework.

Empirical methods estimate CO_2 by extrapolating the sparse ship based CO_2 measurements using satellite observable proxies. This approach has allowed for a better understanding of the drivers of CO_2 by providing improved spatial and temporal resolution of the variability. Landschützer et al. (2015) ~~used~~showed, using an artificial neural network (ANN~~) to show~~), that ~~the~~there was significant strengthening of ~~the~~ Southern Ocean CO_2 uptake during the period 2000-2010 ~~is part of a decadal internal variability in the natural CO_2 flux dynamics.~~. The authors found that the strengthening sink was not due to changes in overturning circulation associated with wind stress as suggested in other studies (Lenton and Matear, 2007; Lovenduski et al., 2007; Lenton et al., 2009; DeVries et al., 2017). Rather, they suggested that atmospheric circulation has become more zonally asymmetric since the mid 2000's. This led to an oceanic dipole of cooling and warming whose net impact together with changes in the DIC/TA (Dissolved Inorganic Carbon/Total Alkalinity) was to increase the uptake of CO_2 (Landschützer et al., 2015). During this period, in the Atlantic basin, southward advection reduced upwelled DIC in surface waters overcoming the effect of the concomitant warming in the region. Conversely, in the Eastern Pacific sector of the Southern Ocean, ~~stronger~~strong cooling overwhelmed increased upwelling (Landschützer et al., 2015). Munro et al. (2015) supported this mechanism, with data from the Drake Passage showing that ΔpCO_2 decreased between 2002 and 2014.

In a subsequent study Landschützer et al. (2016) proposed that interannual variability of CO_2 in the Southern Ocean is tied to the decadal variability of the Southern Annular Mode (SAM) – the dominant

mode of atmospheric variability in the Southern Hemisphere (Marshall, 2003). This concurs with previous studies, which suggested that the increase in the SAM during the 1990's resulted in the weakening of the Southern Ocean sink (Le Quéré et al., 2007; Lenton and Matear, 2007; Lovenduski et al., 2007; Lenton et al., 2009). The work by Fogt et al., (2012) bridges the gap between the proposed asymmetric atmospheric circulation of Landschützer et al. (2015) and the observed correlation with the SAM of Landschützer et al. (2016). Fogt et al. ~~Their study shows~~(2012) show that changes in the SAM have been zonally asymmetric and ~~that~~ that this variability is highly seasonal, thus amplifying or suppressing the amplitude of the seasonal mode.

Assessing the changes through a seasonal framework may thus help shed light on the drivers of CO_2 in the Southern Ocean. Southern Ocean seasonal dynamics suggest that the processes driving pCO_2 are complex but with two clear contrasting extremes. In winter, the dominant deep mixing and entrainment processes are zonally uniform driving an increase in pCO_2 with the region south of the Polar Front (PF) becoming a net source and weakening the net sink north of the ~~PFZ~~PF (Lenton et al., 2013). In summer, the picture is ~~much~~ more spatially heterogeneous, with ~~NPP~~net primary production being the primary driver of variability (Mahadevan et al., 2011; Thomalla et al., 2011; Lenton et al., 2013). The competition between light and iron limitation results in heterogeneous distribution of Chl-*a* in both space and time, with similar implications for pCO_2 (Thomalla et al., 2011; Carranza and Gille, 2015). The interaction between the large-scale drivers, such as wind stress, surface heating and mesoscale ocean dynamics, are the primary cause of this complex picture (McGillicuddy, 2016; Mahadevan et al., 2012). Some regions of elevated mesoscale and submesoscale dynamics, mainly in the Sub-Antarctic Zone (SAZ) are also characterized by strong intraseasonal modes in summer primary production and pCO_2 (Thomalla et al., 2011~~) and pCO_2 (~~; Monteiro et al., 2015). ~~The magnitudes of these~~ In general, the opposing ~~seasonal processes are large, resulting~~effects of mixing and primary production result in the seasonal cycle being the dominant mode of variability in the Southern Ocean~~.~~ (Lenton et al., 2013).

In this study we examine winter and summer interannual variability ~~in the air-sea fluxes~~ of ~~CO_2~~ΔpCO_2 between 1998 – 2014 ~~through interannual changes in the characteristics of the seasonal mode of both pCO_2 and FCO_2~~ in the Southern Ocean~~. We use an ensemble of empirical estimates of CO_2 that combine *in situ* observations with remotely sensed proxies~~ to ~~perform this analysis~~understand the drivers of long term changes in CO_2 uptake.

2 Empirical methods and data

2.1 ~~Ensemble members~~Empirical methods and data

In this study we ~~made~~ use ~~of~~ three ~~empirical methods combined to an ensemble – these~~machine learning methods ~~are~~ : Random Forest Regression (RFR), Support Vector Regression (SVR) and Self-Organising-Maps Feed-Forward Neural Network (SOM-FFN). RFR and SVR are introduced in Gregor et al. (2017) and SOM-FFN is presented in ~~Gregor et al. (2017). The advantage of an ensemble over~~ Landschützer et al. (2014). In brief, the RFR approach is an ensemble of decision trees that provides non-linear regression by combining many high variance – low bias estimators (Gregor et al., 2017). SVRs are in principle similar to a single hidden layer FFN, with the difference that SVR statistically determines the complexity of the problem, which is analogous to the hidden layer structure that is typically determined heuristically. The SOM-FFN method ~~approach is that a degree of robustness is added to the estimate, assuming that ensembles have unique biases in time and space. The other important assumption we make here is that the majority methods will be correct, while the minority will be biased. The ensemble mean contains five different ΔpCO_2 estimate approaches, shown in Table 1, with low- and high-resolution (1°, monthly and 0.25°, 16-day respectively). The SOM-FFN method is defined by Landschützer et al. (2014) and~~ is a two-step neural network approach ~~(trained with SOCAT v2)~~ that first clusters data (SOM) and then applies a regression model (FFN) to each cluster.

The SVR and RFR implementations used in this study are trained with the monthly by 1° gridded SOCAT v3 dataset (Bakker et al., 2016). ~~. 2014). The low resolution implementations of Support Vector Regression (SVR) and Random Forest Regression (RFR) methods are introduced in Gregor et al. (2017). Note that these are~~The SOM-FFN (v2.2) used in this study was trained with SOCAT ~~v3 data (Bakker et al. 2016). The high-resolution implementations of SVR and RFR used in this study are implemented in the same way as described in Gregor et al. (~~v4 (Landschützer et al., 2017). ~~The high-resolution estimates of ΔpCO_2 are resampled to match the low resolution data in the ensemble.~~

25

Table 1: ~~Five~~Three empirical methods used in the ensemble. RFR~~-LR~~ and SVR~~-LR~~ are described in Gregor et al. (2017). SOM-FFN is from Landschützer et al. ~~(Landschützer et al. 2014~~(2016). SST = sea surface temperature, MLD = mixed layer depth, SSS = sea surface salinity, ADT = absolute dynamic topography, Chl-*a* = Chlorophyll-*a*, $pCO_{2(atm)}$ = fugacity of atmospheric CO_2, $xCO_{2(atm)}$ = mole fraction of atmospheric CO_2, ~~Φ(~~~~α~~(lat, lon) = ~~*N*-vector~~*N*-vector transformations of latitude and longitude, ~~λ(~~~~t~~(day of year) = trigonometric transformation of the day of the year. Note that SOM-FFN uses the de Boyer Montégut et al. (2004) climatology for MLD (dBM2004). The root mean squared errors listed in the last column are for the Southern Ocean from Gregor et al. (2017).

Method	~~Resolution~~	Input variables	RMSE (µatm)
		~~Space~~	~~Time~~
RFR~~-LR~~	~~1.00°~~	~~Monthly~~ SST, MLD, SSS, ADT, Chl-$a_{(clim)}$, $pCO_{2(atm)}$, ~~Φ(~~Φ(lat, lon), *t*(day of year)	~~17.21~~16.45
SVR~~-LR~~	~~1.00°~~	~~Monthly~~ SST, MLD, SSS, ADT, Chl-$a_{(clim)}$, $pCO_{2(atm)}$, ~~Φ(~~Φ(lat, lon), *t*(day of year)	~~21.73~~ 24.04
SOM-FFN	~~1.00°~~	~~Monthly~~ SST, ~~MLD~~$MLD_{dBM2004}$, SSS, Chl-*a*, $xCO_{2(atm)}$	~~15.45~~14.84
~~RFR-HR~~	~~0.25°~~	~~16-day~~ ~~SST, MLD, SSS, ADT, Chl-$a_{(clim)}$, $pCO_{2(atm)}$~~	~~12.58~~
~~SVR-HR~~	~~0.25°~~	~~16-day~~ ~~SST, MLD, SSS, ADT, Chl-$a_{(clim)}$, $pCO_{2(atm)}$, Φ(lat, lon), *t*(day of year)~~	~~19.18~~

Table 1 ~~also~~ shows the proxy variables used for each of the methods. ~~The sources for the proxy variables are consistent for all methods ensuring a fair comparison. This is particularly important for the assimilated model variables, mixed-layer depth (MLD) and sea~~Sea surface salinity (SSS) and mixed layer depth (MLD) for SVR and RFR are from Estimating the Circulation and Climate of the Ocean, Phase II ($ECCO_2$) (Menemenlis et al~~.~~., 2008). ~~Choosing to~~The use ~~different~~ of these assimilative modelled products may in some cases produce results that are unrealistic. This may have influenced the use of the de Boyer Montégut et al. (2004) MLD climatology in the SOM-FFN, where $ECCO_2$ was used in previous iterations of the product. The trade-off of using the climatology is that no changes in MLD are taken into account. We acknowledge that using different proxy variables could result in ~~data driven differences (from the same variable).~~different ΔpCO_2 estimates, but comparing the different products is beyond the

scope of this study. Other data sources that are consistent between methods are: sea surface temperature (SST) ~~(~~and sea-ice fraction by Reynolds et al. (2007), Chlorophyll-*a* (Chl-*a*) ~~(~~by Maritorena and Siegel (2005), absolute dynamic topography (ADT) ~~(~~by Duacs~~),~~, xCO_2 (CDIAC, 2016) with $pCO_{2(atm)}$ calculated from interpolated xCO_2 using NCEP2 sea level pressure (Kanamitsu et al~~. 2002).~~., 2002). In the case of Chl-*a* for SVR and RFR, Gregor et al. (2017) filled the cloud gaps with climatological Chl-*a*. Note that ADT coverage is limited to regions of no to very low concentrations of sea-ice cover, thus estimates for SVR and RFR methods do not extend into the ice covered regions during winter. Our analyses are thus limit to the regions without ice cover.

Seasonality of the data is preserved by transforming the day of the year (j) and is included in both SVR and RFR analyses:

$$t = \begin{pmatrix} \cos\left(j \cdot \frac{2\pi}{365}\right) \\ \sin\left(j \cdot \frac{2\pi}{365}\right) \end{pmatrix} \quad (1)$$

Transformed coordinate vectors ~~were~~are passed to SVR only ~~SVR~~ using n-vector transformations of latitude (λ) and longitude (μ) (Gade, 2010; Sasse et al~~.~~., 2013), with n containing:

$$N = \Phi \begin{pmatrix} \sin(\lambda) \\ \sin(\mu) \cdot \cos(\lambda) \\ -\cos(\mu) \cdot \sin(\lambda) \end{pmatrix} \quad (2)$$

~~**2.2 Air-sea CO_2 fluxes**~~

~~Air-sea CO_2 fluxes are calculated with:~~

~~$$FCO_2 = k_w \cdot K_0 \cdot (pCO_2^{sea} - pCO_2^{atm}) \cdot (1 - [ice]) \quad (3)$$~~

~~The gas transfer velocity (k_w) is calculated using a quadratic dependency of wind speed with the coefficients of (Wanninkhof et al. 2009). Wind speed is calculated from the u and v vectors ($\sqrt{u^2 + v^2}$) of the Cross-Calibrated Multiplatform Product v2 (Atlas et al. 2011). Coefficients from Weiss (1974) are used to calculate K_0 and ΔpCO_2 is estimated by the empirical models. The effect of sea-ice cover on CO_2 flux is treated linearly (Butterworth and Miller 2016): the fraction of sea ice cover ([ice]) is converted to fraction of open water by subtracting one as shown in Equation (3).~~

Wind speed, while not used in the empirical methods, is used in the assessment of the drivers of CO_2. We use CCMP v2, which is an observation based product that combines remote sensing, ship and weather buoy data (Atlas et al., 2011). Swart et al. (2015a) compared a number of wind reanalysis products with CCMP v1 (where CCMP was the benchmark). The authors found that the many of the reanalysis products had spurious trends, particularly in the Southern Hemisphere where data is sparse. Our choice of CCMP,

which is based on observations, is thus one that aims to minimise the assumptions that are otherwise made by reanalysis products.

2.2 Uncertainties

The machine learning approaches used in this study are by no means able to estimate ΔpCO_2 with absolute certainty. To account for the uncertainty we use the same approach as Landschützer et al. (2014) to calculate total errors for each of the methods:

$$\boldsymbol{e}_{(t)} = \sqrt{e_{meas}^2 + e_{grid}^2 + e_{map}^2} \quad (3)$$

where $e_{m(t)}$ is the total error associated with a method (m); e_{meas} is the error associated with SOCAT measurements, which is fixed at 5 µatm (Pfeil et al., 2013); e_{grid} is the 5 µatm error associated with gridding the data into monthly by 1° bins (Sabine et al., 2013). Lastly e_{map} is the root mean squared error (RMSE) calculated for each method as shown in Table 1 taken from Gregor et al. (2017).

These errors are used to calculate the average "within-method" error as defined by Gurney et al. (2004):

$$\mathrm{E}_w = \sqrt{\frac{1}{M} \cdot \sum_{m=1}^{M} (e_{m(t)})^2} \quad (4)$$

where $e_{m(t)}$ is the method specific error as defined in Equation 1 and M is the number of methods (3 in this case). For a measure of the difference between methods we use the "between-method" approach used in Gurney et al. (2004):

$$E_b = \sqrt{\frac{1}{M} \sum_{m=1}^{M} (S_m - \bar{S})^2} \quad (5)$$

where S_m is the method estimate of ΔpCO_2 and $\bar{S}$ is the mean of the methods. This is analogous to the standard deviation (for a known population size). We later use an adaptation of this metric as a threshold to determine the confidence around anomalies.

2.3 Regional Coherence Framework

Southern Ocean CO_2 is spatially heterogeneous both zonally and meridionally (Jones et al. 2012). In order to understand this heterogeneity we used the three southernmost biomes defined by Fay and McKinley (~~2017~~2014a) as done in Rödenbeck et al. (2015). From north to south these are: ~~sub-tropical~~subtropical seasonally stratified (STSS), sub-polar seasonally stratified (SPSS), seasonally ice covered region (ICE). These three biomes are comparable to the SAZ, PFZ and MIZ respectively and will be used throughout the rest of the study. The Southern Ocean is further split into basins where the boundaries are defined by lines of longitude (70°W : Atlantic : 20°E : Indian : 145°E : Pacific : 70°W).

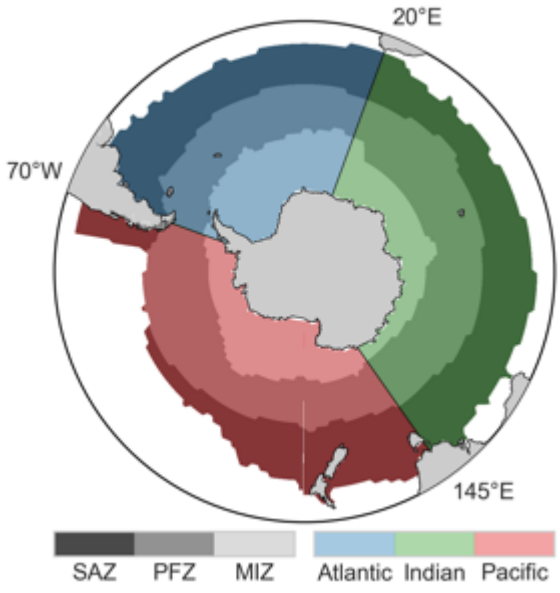

Figure 1: A map showing the regions used throughout this study. The three biomes, SAZ, PFZ and MIZ used in this study are defined by Fay and McKinley (~~2014~~2014a). The regions are also split by basin ~~with boundaries shown above the map~~.

3 Results and discussion

~~In this section~~Here we present and discuss the ~~data~~results. The first section examines the ~~variability~~uncertainties of ~~between~~ the ensemble and its members ~~to understand the potential limitations of the dataset~~. We then look at the seasonal cycle of the ensemble mean in time and space. This is done to lay the foundation ~~knowledge~~ for the interpretation of the results when assessed with the regional framework~~, which is the following section.~~. In the regional interpretation the data is decomposed into nine regions as shown in Figure 1. ~~The section that follows sets out to make sense~~Lastly we implement a seasonal decomposition of the ~~trends~~estimates to interpret the drivers of the changes observed in ~~the regional decomposition.~~ ΔpCO_2.

3.1 Ensemble member performance and variability

~~In this section we discuss the performance and variability~~**Table 2: A regional summary of the ~~ensemble members.~~errors for the different models. Note that the propagated errors are calculated as shown in equation (3) where the measurement and gridding errors are assumed to be constant at 5 µatm each (Pfeil et al., 2013; Sabine et al., 2013). The ~~individual ensemble member~~ within-model and between model errors are calculated using equations (4) and (5) respectively.**

Biome	Propagated errors (µatm)			Within model (µatm)	Between model (µatm)
	SVR	RFR	SOM-FFN		
SAZ	17.48	14.50	12.30	14.91	4.88
PFZ	15.94	12.71	13.09	13.99	4.78
MIZ	36.38	24.53	22.46	28.46	10.81
Southern Ocean	**25.06**	**17.91**	**16.44**	**20.16**	**6.79**

We use the RMSE scores ~~are~~ as presented in Gregor et al. (2017) with abbreviated results shown in Table 1. The ~~RFR-HR is~~SOM-FFN method has the best ~~performing member, with~~ score (14.84 µatm). SVR

scores the lowest ~~RMSE (12.58 µatm). The SVR members score the lowest (21.73 and 19.18 µatm for LR and HR respectively~~(24.04 µatm), but ~~were~~was still included due to the method's sensitivity to sparse data, which is favourable to the poorly sampled winter period (Gregor et al. 2017). This compliments the RFR ~~methods~~method, which ~~score~~scores well (~~12.58 and 17.21 µatm for HR and LR respectively~~16.45 µatm), but ~~are~~is prone to being insensitive to sparse data (Gregor et al. 2017). ~~The SOM-FFN member has~~These RMSE scores are used to calculate the ~~best of the low-resolution scores (15.45 µatm). However, this is because the SOM-FFN is tested with SOCAT v2 data rather than SOCAT v3,~~total errors for each method and region using equation (3) where the ~~latter has a larger standard deviation (32.85 and 36.27 µatm respectively). When RFR-LR and SVR-LR~~measurement and mapping errors are ~~tested with the SOCAT v2 dataset, the RMSE scores are 15.15 and 19.82 µatm respectively~~both 5 µatm each (Pfeil et al., 2013; Sabine et al., 2013). These results are shown in Table 2.

Total errors are used to calculate the within-method error, which is an estimate of the combined total errors of the three machine learning methods (equation 4). The between-method errors are the mean of the standard deviation between the methods (equation 5). The within-method errors are much larger than the between-method errors (Table 2). However, the within-method errors are normally distributed and are mechanistically consistent (Gregor et al., 2017).

This allows us to observe changes that are smaller than the within-method error. The between-method error (shown in Figures 2d) serves as a better measure of whether observed variability is more than statistical noise as it incorporates the three methodologically different approaches.

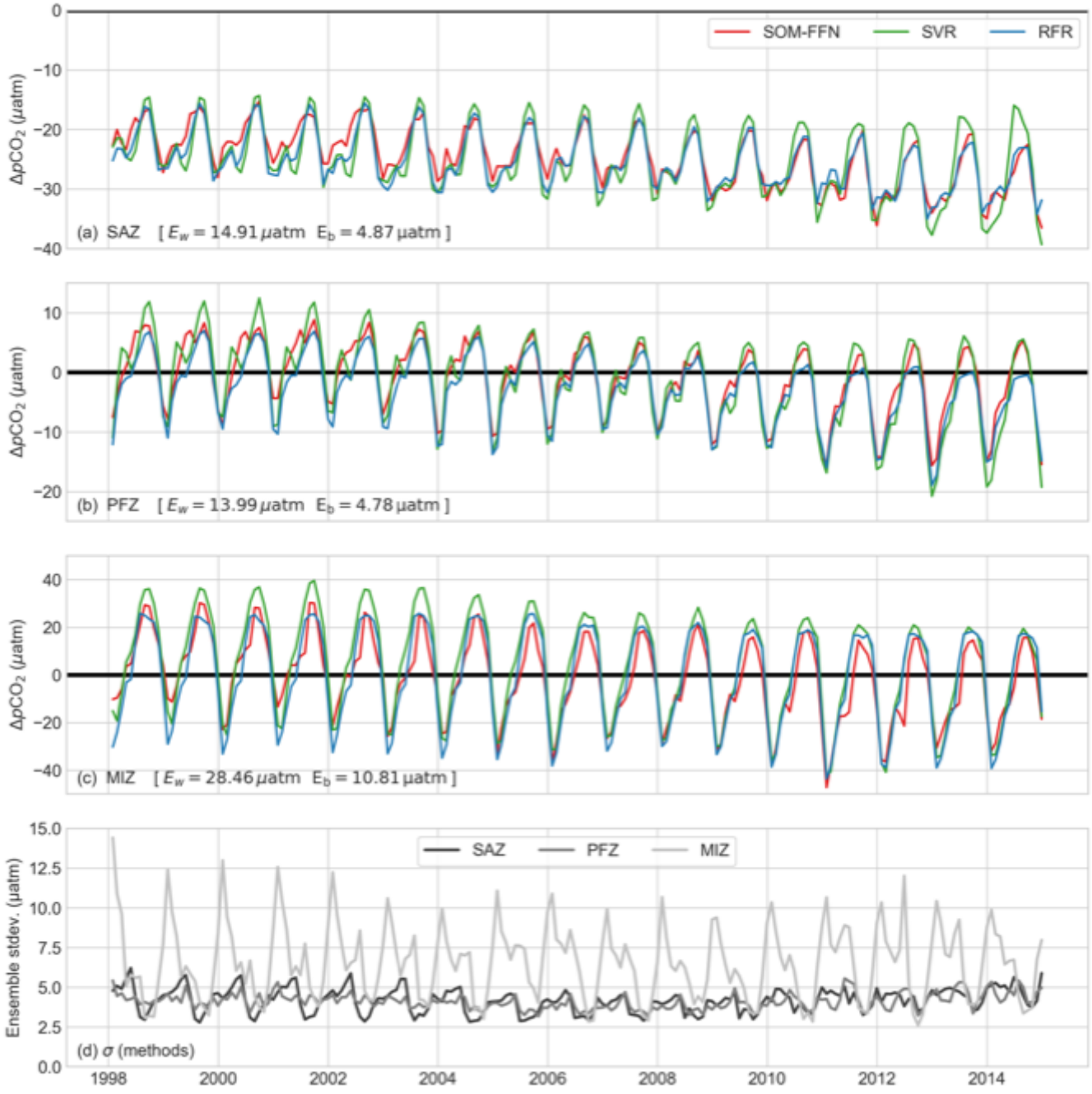

Figure 2: Time series of the five ensemble members for each biome as defined by Fay and McKinley (~~2014~~2014a): (a) SAZ, (b) PFZ, (c) ~~AZ~~MIZ. (d) shows the standard deviation between ensemble members for the three biomes~~.~~ which is analogous to the between-model error (equation 5). The ~~SOM-FFN data ends at the end~~within-method (E_w) and between-method (E_b) errors are shown for each biome. For a more detailed breakdown of ~~2011. This is indicated in (d) by~~ the ~~dashed line.~~ errors see Table 2.

Figure 2 shows the ΔpCO_2 time series ~~of the~~for each of the methods for the three Southern Ocean biomes ~~as defined by Fay and McKinley (2014).~~. The methodological and data driven differences between each of the ~~approaches~~methods have been addressed in Gregor et al. (2017). In general, there is good agreement amongst the methods with a few notable exceptions. In the SAZ (Figure 2a) ~~The~~the SOM-FFN differs from ~~all~~the other methods for summer and autumn from 1998 to 2008. Gregor et al. (2017) attributed this difference to the clustering step ~~used by~~in the SOM-FFN that ~~created large~~creates discrepancies in the Atlantic sector. The SVR ~~LR~~ method overestimates the seasonal amplitude ΔpCO_2 relative to the other

methods for ~~winter~~ 2012 to 2014. In the PFZ (Figure 2b), the SVR ~~methods (LR and HR) overestimate~~overestimates ΔpCO_2 relative to the other methods during winter from 1998 to 2004, likely due to the sensitivity to sparse winter data. ~~The spread of data in the AZ is much larger than~~ These differences contribute to the ~~two other regions, but the impact on the fluxes is reduced due to ice cover during winter (Ishii et al. 1998; Bakker et al. 2008; Butterworth and Miller~~between-method error. ~~2016).~~

The seasonal amplitude

~~*Figure 3: The mean spatial standard deviation (a) of the ensemble members (SVR-LR, SVR-HR, RFR-LR, RFR-HR and SOM-FFN) is shown to represent the "noise" of the ensemble mean. The "signal" (b) is calculated as the mean difference between the minimum and maximum values of the annually averaged ΔpCO_2. This shows the signal that needs to be detected by the ensemble. The signal to noise ratio (c) shows regions where the confidence in the ensemble estimate is large, where darker shows higher confidence.*~~

~~The results from Figure 2(a-c) are summarised with the standard deviation of the ensemble members over time (Figure 2d) and space (Figure 3). As noted, the AZ (Figure 2c) has the largest disagreement amongst methods shown by map (Figure 3a) and the differences between the solid and dashed lines in Figure 2d, particularly during summer and autumn. This is likely due to the inability of the methods to accurately capture the larger intra-seasonal variability and patchiness in the AZ where the rapid reduction of pCO_2, due to melting sea ice leads to patchy pCO_2 distributions (Bakker et al. 2008; Chierici et al. 2012). The ensemble members are more coherent in the SAZ and PFZ.~~

~~In order to ascertain a degree of coherence and confidence in the ensemble we show the signal to noise ratio in Figure 3c. We define the signal as the largest difference in the trend for a particular point. This is calculated from the largest difference of annual averages of ΔpCO_2. The noise is the mean standard deviation of ensemble member estimates. A large signal to noise ratio (Figure 4c) is indicative of a large trend signal compared to the variability of the ensemble. While signal to noise ratio is > 1 for the entire domain, there are regions where the ratio is < 2: parts of the Atlantic sector of the SAZ and the Indian sector of the PFZ.~~

~~With the established baseline of confidence in the ensemble, the ensemble mean of ΔpCO_2 can be assessed. The seasonal cycle is the strongest mode of ΔpCO_2 variability in the Southern Ocean (Lenton et al. 2013). It is therefore important that the ensemble mean is understood in the context of our current understanding of the seasonal cycle.~~

of ΔpCO_2 in the MIZ is much larger than the two other regions. However, this amplitude is likely to be dampened by ice cover (Ishii et al., 1998; Bakker et al., 2008; Butterworth and Miller, 2016). Note that in this study, we do not include regions with sea-ice cover to ensure consistency between methods. Calculated fluxes for this methodologically reduced region will thus under-represent the fluxes of the full extent of the MIZ. We thus exclude the MIZ for the remainder of the study.

Figure 2(d) shows the time evolution of between-method errors for each biome. This panel highlights the seasonality of the data, specifically the increased heterogeneity of ΔpCO_2 in summer and the impact that this has on ΔpCO_2 estimates This is due to the more complex competing processes affecting pCO_2 during summer. To gain a better understanding of the seasonal processes we look at the mean state of each season to characterise the drivers of opposing fluxes.

3.2 Ensemble seasonal cycle

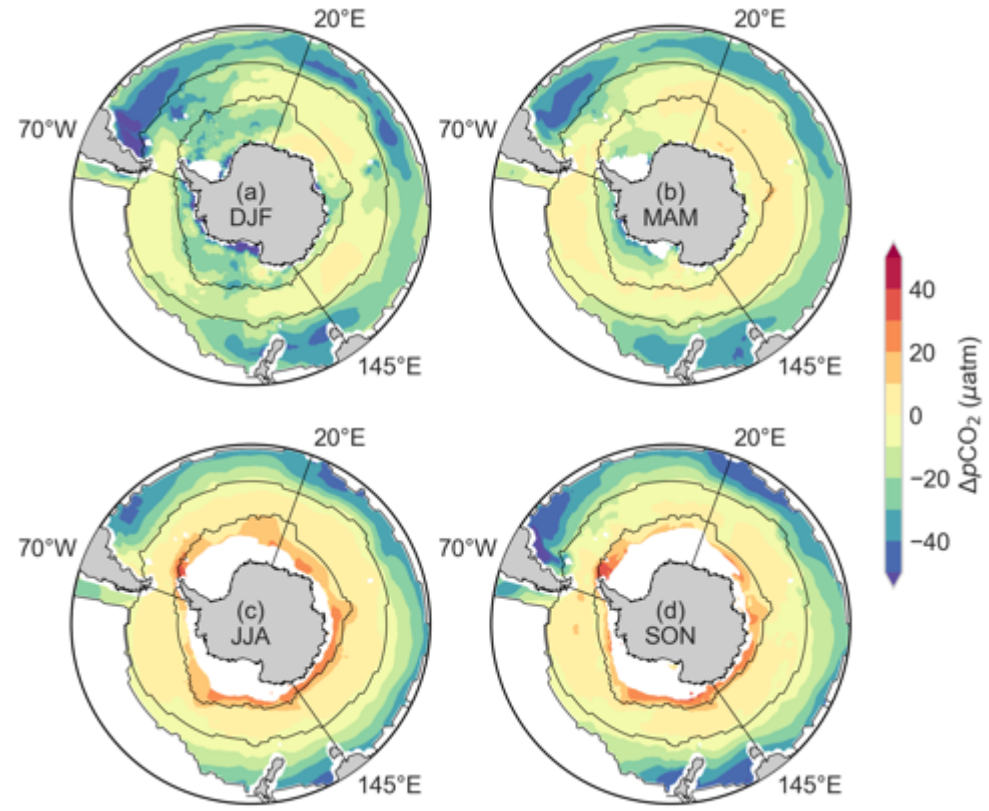

Figure 43: The mean seasonal states of ΔpCO_2 of the empirical ensemble mean]{Seasonal averages of pCO_2 for the ensemble of ΔpCO_2. These are shown for (a) summer, (b) autumn, (c) winter and (d) spring. The black contour lines show the SAZ, PFZ and AZMIZ from north to south as defined by Fay and McKinley (20142014a).

The seasonal cycle of the ΔpCO_2 for each biome (Figure 2a-c and Figure 4a3a-c) is coherent with expected seasonal processes based onreported in the literature (Metzl et al., 2006; Thomalla et al., 2011; Lenton et al., 2012; Lenton et al., 2013). In all biomes, uptake of CO_2 is stronger during summer than in winter giving rise to the strong seasonal cycle. This is due to the opposing influences of the dominant winter and summer drivers, partially damped by the seasonal cycle of temperature (Takahashi et al., 2002; Thomalla et al., 2011; Lenton et al., 2013). The dominant processes of mixing and entrainment in winter resultsresult in increased surface pCO_2 and thus outgassing (Takahashi et al., 2009; Lenton et al., 2013; Rodgers et al., 2014). In summer, stratification also allows for increased biological production and the consequent uptake of CO_2, thus reducing the entrained winter DIC and associated pCO_2 (Bakker et al., 2008; Thomalla et al., 2011). However, stratification typically limits entrainment, but does not exclude

the occurrence of entrainment during periods of intense mixing driven by storms~~, which~~. This has an impact on ~~both~~ primary productivity, DIC and pCO_2 (Lévy et al~~.~~., 2012; Monteiro et al~~.~~., 2015; Nicholson et al~~.~~., 2016; Whitt et al~~.~~., 2017).

The SAZ (Figure 2a) is a continuous sink where summer uptake (Figure ~~4a~~3a) is enhanced by biological production and winter (Figure ~~4e~~3c) mixing results in a weaker sink (Metzl et al~~.~~., 2006; Lenton et al~~.~~., 2012; Lenton et al~~.~~., 2013). ~~These~~The same processes produce a similar seasonal amplitude in the PFZ (Figure 2b), but ~~the seasonal fluxes are~~stronger upwelling and weaker biological uptake result in a positive shift of the mean. This results in an opposing~~: a sink in~~ net summer ~~(< 0 µatm)~~sink and ~~a source in~~ winter ~~(> 0 µatm).~~source. However, this is according to the mean state in the PFZ and winter estimates of ΔpCO_2 do in fact approach 0 µatm toward the end of the time series (Figure 2b). The ~~AZ~~MIZ has the strongest seasonal cycle due to upwelling of CO_2 during winter and strong biological uptake in summer. However, much of this is dampened by sea ice cover during winter and weaker winds during summer (Ishii et al~~.~~., 1998; Bakker et al~~.~~., 2008).

~~It~~Apparent also from Figure 3 is ~~important to note~~ that, over and above the latitudinal gradient, ΔpCO_2 is zonally asymmetric within each biome~~, particularly~~ during summer (Figure ~~4a~~3a) when biological uptake of CO_2 increases. Zonal integration of ΔpCO_2 ~~and FCO_2~~ could thus dampen magnitudes of regional ~~signals~~ΔpCO_2. A regional approach is therefore needed to examine the regional characteristics of seasonal and interannual variability of ΔpCO_2 and ~~FCO_2 and~~ to understand ~~their~~its drivers.

3.3 Regional ΔpCO_2 ~~and FCO_2 Variability: Zonal~~variability: zonal and basin contrasts

Here ΔpCO_2 ~~and FCO_2 are~~is decomposed into nine domains by biome and basin with the boundaries shown in Figure 1~~.~~, but note only six are shown in Figure 4. The data are plotted as time series for pCO_2 (Figure ~~5) and FCO_2 (Figure 6~~4) showing: ~~the~~ mean annual ~~trends of pCO_2 and FCO_2~~ (black lines), the maximum winter values (red line) and the projected summer minima (dashed red line~~) based on adjusting the winter maxima each year by the mean of the difference between the winter maxima and the summer minima (Figures 5, 6).~~). The projected summer minima ~~implies that there is an~~are calculated by subtracting the mean seasonal amplitude from the winter maxima (Figure 4, with air-sea CO_2 fluxes shown in Figure S3). The projected summer minima sets the expectation that summer ΔpCO_2 is dependent on, but not restricted to, the baseline set by ~~the~~ winter ~~maxima~~. Differences between the ~~ensemble~~ summer minima and projected minima are highlighted with green and blue patches, highlighting periods of decoupling between summer and winter interannual variability. The green areas indicate periods of strong uptake (relative to winter) that enhance the mean uptake of CO_2~~.~~ and amplify the seasonal cycle. Conversely, blue areas show periods where weak summer uptake (relative to winter) offsets winter

~~trend~~outgassing, thus reducing the mean ~~trend.~~ ΔpCO_2 as well as supressing the amplitude of the seasonal cycle (Figure 4).

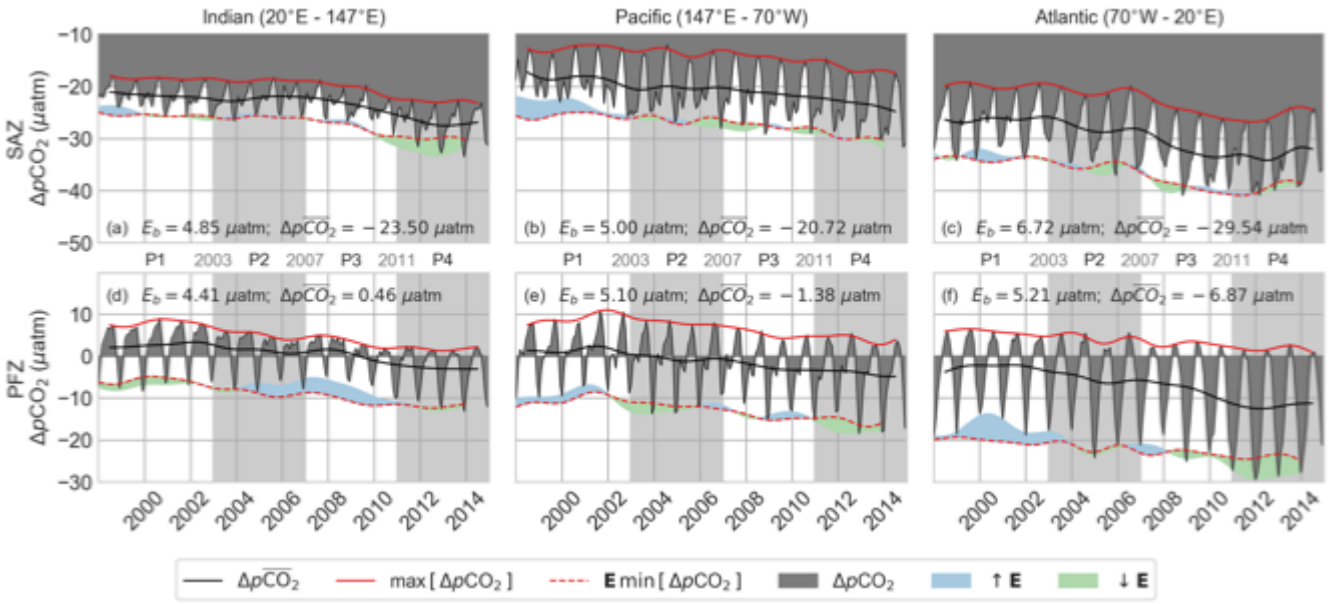

Figure ~~5~~4: Figures (a-~~i~~f) show ΔpCO_2 (dark grey) ~~and (j-r) show FCO_2 (dark grey)~~ plotted by biome (rows) and basin (columns). Biomes are defined by Fay and McKinley (~~2014~~2014a). The solid red line shows the maximum for each year (winter outgassing) and the dashed line shows the same line less the average ~~difference between the minimum and maximum~~seasonal amplitude – this is the expected amplitude. The shaded blue (green) area shows when the annual minimum is less (greater) than the expected amplitude. ~~ΔpCO_2~~ E_b is the average between-method error and $\Delta p\overline{CO}_2$ is the average for ~~plots (g-i) was normalised to sea ice cover, but under ice ΔpCO_2 estimates were still used to find the expected amplitude.~~the entire time series. Light grey shading in (a-~~i~~f) shows the ~~proposed~~ periods used in Figure ~~9 and~~Figure ~~10 Light grey shading in (j-r) shows the "saturation" period (1998 to 2001) and the "reinvigoration" period (2002 to 2011).~~5 and Figure 6.

The data for ΔpCO_2 ~~and FCO_2 (Figures 5 and 6), show~~(Figure 4) shows that the Southern Ocean sink strengthened from 2002 to 2011 in all domains, a period identified as the *reinvigoration* by Landschützer et al. (2015). This was preceded by a period of a net weakening sink in the 1990's referred to as the *saturation* period after Le Quéré et al. (2007). ~~These two periods are highlighted by the grey fill in Figure 6. The saturation of the Southern Ocean CO_2 sink is not as strong in the ensemble, occurring in only five of the nine domains (see the positive trend slopes between 1998 and 2002 in Figure 6).~~ In the ~~last~~ period ~~(~~from 2012 to 2014~~) of the ensemble,~~ three domains (Figure 4a,c,f) go from growing uptake to reducing uptake; however, our confidence in the ~~increasing trends from 2012 to 2014~~ changing trend is low due to lack of coherence between methods (Figure 2a,b) and only three years of data, with ~~very sparse~~few data in 2014.

~~Importantly, these~~A key feature of Figure 4 is that the mean interannual ~~trends are~~variability is the ~~integrated~~net effect of decoupled seasonal modes of variability~~.~~ for summer and winter. This is particularly evident in the PFZ (Figures ~~5d~~4d-f). Here, and in the other biomes, ~~there is a~~the net

strengthening of the CO_2 sink ~~due~~ is mainly linked to a reduction of ΔpCO_2 in winter ~~on roughly a decadal mode~~ for the majority of the time series. This corresponds with the findings of Landschützer et al. (2016), who linked the ~~decadal variability~~reinvigoration to the decadal variability of the Southern Annular Mode (SAM) – the dominant mode of atmospheric variability in the Southern Hemisphere (Marshall, 2003). In ~~comparison~~contrast, summer ΔpCO_2 variability is ~~sub-decadal or~~ shorter (roughly 4 – 6 years~~,~~), thus ~~impacting the short term~~providing inter-annual modulation of longer time-scale winter variability ~~of the annually integrated trend~~. This is demonstrated well in the Indian sector of the PFZ where a decrease in winter ΔpCO_2 from 2002 to 2011 is offset by weakening of the summer sink from 2006 to 2010 (Figure ~~5d, 6d~~4d). Similarly in the Atlantic and Pacific sectors of the ~~SAZ and~~ PFZ ~~strong~~ decoupling occurs from ~2011 to the end of 2014 with a rapid increase in the strength of the summer sink.

The mean amplitude of the seasonal cycle of ΔpCO_2, the mean difference between the summer minima and the winter maxima, is ~~perhaps~~ a better means of understanding the ~~magnitude~~strength of the seasonal drivers ~~for each domain~~ than the mean ΔpCO_2 ~~(Table A1).~~. For example the Atlantic sectors of the SAZ and PFZ (Figures ~~5c~~4c,f) have the strongest seasonal variability (~~20.57~~14.11 and ~~27.67~~25.83 µatm respectively). This contrasts the relatively weak seasonal amplitude in the Indian sector of the Southern Ocean which has mean amplitudes of ~~8.85~~7.06 and 13.~~31~~64 µatm for the SAZ and PFZ respectively (Figures ~~5b~~4b,e). This contrast can also be seen by comparing the mean seasonal maps of ΔpCO_2 in Figures ~~4a~~3a and ~~4e~~3c. In summer, strong uptake in the eastern Atlantic sector of the southern ocean is indicative of large biological drawdown of CO_2 by phytoplankton (Thomalla et al~~.~~., 2011). Conversely, relatively low primary production in the Indian sectors of the SAZ and PFZ result in a small seasonal amplitude (Thomalla et al~~.~~., 2011). This large discrepancy in biological primary production is related to the availability of iron, a micronutrient required for photosynthesis. The lack of large land masses, a source of iron, in the Indian sector of the Southern Ocean could be a contributing factor to the lack of biomass (Boyd and Ellwood, 2010; Thomalla et al~~.~~., 2011).

~~The seasonal amplitude in the AZ is much larger due to strong contrast of the upwelling of CO_2 rich deep water contained beneath winter sea ice and the strong biological drawdown in the beginning of summer (Ishii et al. 1998, Bakker et al. 2008). Rapid stratification and iron supply by melting sea ice provide the environment for phytoplankton to proliferate in the AZ. This results in large seasonal amplitudes of 46.72, 75.46 and 64.29 µatm for the Indian, Pacific and Atlantic.~~

~~The air – sea fluxes of CO_2 (FCO_2) have decadal trends that are coherent with the pCO_2 (Figure 6), but there are notable differences that emerge from the impact of wind on the rate of exchange as well as the surface area of each domain (Figure A1). Most prominent are the changes in the seasonal cycle and the~~

mean seasonal sink of FCO_2 relative to pCO_2 with amplification in the Indian sector (Figures 5a,d and 6a,d) and weakening in the Atlantic Ocean (Figures 5c,f and 6c,f) of the Southern Ocean. The Indian sector of the SAZ (Figure 6a) dominates the uptake of CO_2 with an annual mean flux of -0.25PgC yr-1 compared to -0.19 and -0.17 PgC yr-1 for the Atlantic and Pacific sectors respectively (where the latter are significantly different with p = 0.01). The seasonality of wind stress (see Figure A1) results in a damped seasonal cycle of FCO_2 in the SAZ and increasing intra-seasonal variability (compared to ΔpCO_2), with stronger winter winds compensating for a weaker ΔpCO_2 gradient (Monteiro et al. 2015).

Figure 6: Figures (a-i) show ΔpCO_2 (dark grey) and (j-r) show FCO_2 (dark grey) plotted by biome (rows) and basin (columns). Biomes are defined by Fay and McKinley (2014). The solid red line shows the maximum for each year (winter outgassing) and the dashed line shows the same line less the average difference between the minimum and maximum – this is the expected amplitude. The shaded blue (green) area shows when the annual minimum is less (greater) than the expected amplitude. ΔpCO_2 for plots (g–i) was normalised to sea ice cover, but under ice ΔpCO_2 estimates were still used to find the expected amplitude. Light grey shading in (a-i) shows the proposed periods used in Figure 9 and Figure 10 Light grey shading in (j-r) shows the "saturation" period (1998 to 2001) and the "reinvigoration" period (2002 to 2011).

This contrasts the PFZ, where opposition of summer uptake and winter outgassing of CO_2 is amplified by stronger wind stress (Figure 6d–f). Interannual variability is also enhanced, particularly during winter in the Indian sector of the PFZ, where a reduction in outgassing of 0.18 PgC yr^{-1} is observed. The decoupling between summer and winter FCO_2 also becomes more pronounced in this region (Figure 6d), resulting in a lag in the decreasing trend. In other words, the trend of FCO_2 for the reinvigoration (2002 through 2011: -10.85 PgC yr-1) would have been stronger if the decoupling had not occurred. Similarly, the seasonal decoupling in the Pacific sector of the SAZ and PFZ results in a stronger growing sink from 2012 to 2014. In the Atlantic sector of the SAZ and PFZ the earlier onset of the seasonal decoupling (Figure 5c,f) also means that re-coupling occurs sooner, resulting in a positive flux trend (Figure 6c,f). Lastly, FCO_2 in the MIZ is damped during winter due to ice cover and weaker winds during summer when ΔpCO_2 is low due to the short-lived intense biological uptake of CO_2 (Ishii et al. 1998; Bakker et al. 2008).

3.4 Seasonal deconstruction of interannual variability

Figures 5 and 6 giveFigure 4 gives us insight into the magnitude of FCO_2 and ΔpCO_2 interannual ΔpCO_2 variability as well as the character of these changes; *i.e.* decoupling of decadalinterannual winter and sub-decadal summer interannual modes of variability. This alludes to the factpoint that ΔpCO_2 and FCO_2 areis responding to different adjustments of seasonal large scale atmospheric forcing and/or responses of internal ocean dynamics in the Southern Ocean (Landschützer et al., 2015, 2016; DeVries et al., 2017). In the study by Landschützer et al. (2015) it was advanced that the explanation for the reinvigoration of ΔpCO_2 uptake in the 2000s decade was linked to the net thermal control driven by a response of DIC and temperature to asymmetric atmospheric forcing over the Southern Ocean. More recently, a study by DeVries et al. (2017) proposed that the Southern Ocean uptake was due to the global deceleration of the

~~Meridional Overturning Circulation (MOC). They suggested that the MOC was increasing the oceanic storage and reducing the losses of CO_2 to the atmosphere, particularly in the Southern Ocean. The mechanism proposed by DeVries et al. (2017) is the same as that put forward by Le Quéré et al. (2007) and Lovenduski et al. (2008) amongst others, where the changes in outgassing are related to the strength of the westerly winds over the Southern Ocean. These studies have in linked the wind stress variability to SAM.~~

In order to capture the decoupled short term variability observed during summer, the data are ~~broken~~divided into four interannual periods (P1 to P4~~)~~), where P1 is five years and the remaining periods (P2 to P4) are four years as shown by the light grey fills in Figure ~~5. The first period is the saturation period (P1: 1998 – 2002) by Le Quéré et al. (2007). The second and third periods are informed by the reinvigoration period (2002 through 2011) split around the start of 2007 an early, weaker reinvigoration (P2: 2002 – 2006) and a late, stronger reinvigoration (P3: 2007 – 2011). The last period incorporates the three years of new data (P4: 2012 to 2014).~~4. The small discrepancy in the length of the periods is due to the uneven length of the time series (17 years).

These four periods are too short for trend analyses (Fay and McKinley, ~~2014~~2014b), but the intention here is to identify periods that are short enough to resolve interannual changes ~~in the~~of large~~-~~scale drivers of the winter and summer ~~mean values for~~ pCO_2 ~~and~~ FCO_2 that would otherwise be averaged out over longer periods. We ~~perform an~~then calculate the relative anomaly ~~analysis~~ between each successive period rather than ~~a trend analysis (for which inflections of ΔpCO_2 would be more suitable delimiters). The relative anomalies in~~ an anomaly of the ~~drivers are their differences between two adjacent periods~~mean state (*e.g.* P2 – P1). As a result four periods give rise to three sub-decadal-scale transition anomalies for summer and winter: *A* (P2 – P1), *B* (P3 – P2) and *C* (P4 – P3). We do this separately for each method rather than using the ensemble mean (see S4 for calculations). The mean of the method anomalies for each transition is then taken. These anomalies are considered significant if the absolute estimate of the anomaly is larger than the standard deviation between the methods for each period. These calculations along with plots for the standard deviation between methods are shown in the supplementary materials in S4.

Note that, although only summer and winter anomalies are discussed, it is recognised that autumn and spring could be equally mechanistically important. Winter anomalies of ΔpCO_2, wind stress, SST and MLD are shown in Figure ~~7~~5. Summer anomalies of ΔpCO_2, wind stress, SST and Chl-*a* are shown in Figure ~~8~~6 where MLD, in winter, is replaced with Chl-*a* for summer as it is potentially a more

important driver than the generally shallow ~~MLD in~~ summer MLD (the omitted plots are shown in Figures ~~A2~~S5 and ~~A3~~S6).

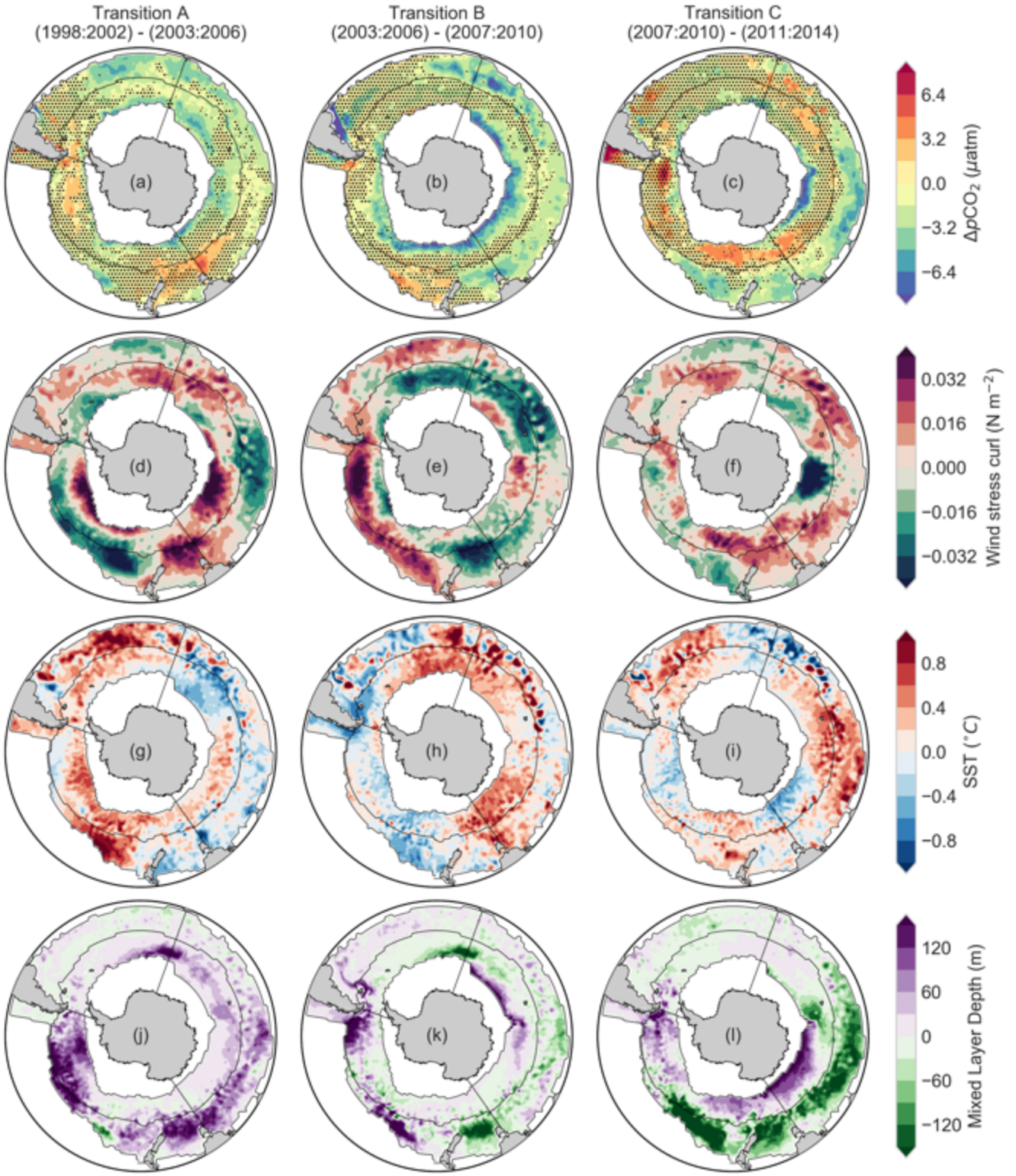

Figure ~~7: Transitions of winter ΔpCO_2, wind stress, SST and MLD]{~~5:**Transitions (relative anomalies) of winter ΔpCO_2 (a-c), wind stress (d-~~e~~f), sea surface temperature (~~f-h~~g-i) and mixed layer depth (~~i-k~~j-l) for four periods ~~(as shown above each column).~~ The thin black lines show the boundaries for each of the nine regions described by the biomes (Fay and McKinley ~~2014) and basin boundaries.~~ , 2014a) and basin boundaries. Regions with dots in (a-c) are where the anomalies are not significant ie: standard deviation of the anomalies between models is greater than the absolute mean of method anomalies as described in equations S1 to S3.**

3.5 Drivers of ~~the decadal~~ winter ~~trends in~~ ΔpCO_2 ~~and FCO_2~~variability

~~There are two features of interest in the anomalies of winter ΔpCO_2 and its drivers (Figure 7). First, there is a zonally asymmetric dipole for wind stress between the Pacific and Indian sectors of the Southern Ocean that dominates transitions A and B. Second, ΔpCO_2, SST and MLD cohere roughly to the spatial variability of wind stress anomalies, mirroring the wind dipole. These features will be expounded on in the paragraphs that follow.~~

We will limit the interpretation of the changes to the regions where the anomaly is larger than the between-method error of anomalies (see S4 for calculations and maps). This masks out large regions, but three key points still arise from the significant anomalies. Firstly, ΔpCO_2 is often spatially roughly coherent with wind stress and the inverse of SST. Secondly, there is a dipole in the wind anomalies in the Indian and Pacific between transitions A and B. This is confirmed by the *u*- and *v*-components of wind shown in the supplementary materials (Figure S5). Lastly, the Indian sector of the Southern Ocean dominates the reinvigoration of the CO_2 sink. These points are now addressed in more detail.

Transition A (~~the transition from P1, the saturation period, to~~ P2~~, the start of the reinvigoration~~ – P1) shows a relative increase of ΔpCO_2 in the east Indian and Pacific sectors of the SAZ – suggesting a delay in the onset of the reinvigoration for these basins. This regional sustained saturation corresponds to a shift towards stronger winds and/or deeper MLDs west of the Tasman Sea (Pacific sector of the SAZ) and surrounds (Figure ~~7d~~5d,j). In contrast, CO_2 uptake in the east Atlantic and west Indian sectors of the SAZ~~, and the south-eastern Indian sector of the PFZ show a reinvigoration of CO_2 uptake. In the central Pacific, weaker wind stress (green in Figure 7d)~~ start to strengthen, which roughly corresponds with ~~relative warming and shoaling or stagnation of MLD. This is consistent with an invigoration of the Southern Ocean CO_2 sink (P1 – P2: 1998 – 2007) initiated by a weakening of the mean westerly wind stress in the Pacific and W Indian Oceans, which we are suggesting, reduced winter entrainment and possibly upwelling of CO_2-rich deep waters (Marshall, 2003; DeVries et al. 2017).~~the weaker winds.

Transition B, ~~which corresponds to anomalies between~~(P3 – P2~~ to P3 (the two reinvigoration periods~~), is characterized by ~~an~~ a further intensification of the invigoration of ΔpCO_2 ~~(-ve~~(negative shift) ~~in all basins, but particularly~~primarily in the Indian basin (Figure ~~7b). This~~5b). Once again the strengthening of the CO_2 uptake corresponds with weaker wind stress, a warming trend in surface waters and shoaling MLDs in the ~~SE~~eastern Atlantic and Indian Ocean sectors ~~in~~of the ~~winter~~SAZ and PFZ (Figure ~~7b~~5b,e,h,k). ~~In the Pacific, the~~The opposing effects of the dipole are~~:~~ observed east of New Zealand where stronger wind stress, deeper MLD, and cooler surface waters~~. These changes are associated~~ corresponds with ~~the~~

persistence of a neutral to weak reduction of positive shift in ΔpCO_2 compared to the Indian sector. All the changes in transitions A and B are coherent to changes in the Pacific–Indian wind stress dipole..

In transition C (P4 – P3: 2012 - 2015), when we propose the invigoration trend starts to weaken,), ΔpCO_2 sink strengthens further in the northern and southern extremes of the east Indian and west Pacific basins, albeit in a more spatially heterogeneous way. In the Atlantic sector the previous invigoration trend reverses completely and the CO_2 sink in the winter is shown to weaken. This negative shift corresponds well with strong shoaling of the MLD (Figure 7b,e5l). The previously well characterizedwest Pacific–Indian dipole is not apparent, suggesting that transition A and B capture well established phases in the decadal variability, while transition C may be capturing a transition into the following phase sector of the PFZ shows a positive shift in ΔpCO_2, which could take the system back to the same configuration as P1. The notion that this period is a snapshot between two distinct phases is supported by the relatively heterogeneous spatial structure of is coherent with an increase in the wind stress in both the Atlantic and Indian Oceansand deepening MLD.

3.5.1 Wind dominated interannual variability of pCO_2 in winter

WeBased on the observations outlined above, we propose that the interannual variability of seasonal the regional (basin-scale) characteristics of winter wind stress in winter may be the dominant driver of the saturation and reinvigoration periods. Moreover, the suggested Pacific–Indian wind dipole may be linked to the decadal variability of ΔpCO_2 observed in the Southern Ocean (Landschützer et al. 2016).

IncreasingThese findings suggest that increasing or decreasing interannual winter wind stress variability impacts ΔpCO_2 (and thus FCO_2) by driving strongerchanges in turbulent mixing. that set the magnitudes of winter entrainment. In the transition to and during winter, this mixing is associated with changes in rates of heat loss resulting in athat drive loss of buoyancy or weaker stratification (Abernathey et al.,, 2011). Weaker buoyancy facilitates deepening of the MLD, thus entraining DIC-rich deep waters (Abernathey et al.,, 2011; Lenton et al.,, 2013). Conversely, decreased wind stress and mixing during winter (on seasonal or interannual time scales) reduces the rate of heat loss (represented as warm anomalies in Figure 75). This results in stronger stratification and shallower winter MLD limits entrainment of DIC, which strengthens the CO_2 winter disequilibrium and leads to a stronger CO_2 sink anomaly (Figure 7). This is5). These are the mechanismmechanisms that resultswe propose result in decreasing or increasing fluxes with interannual and basin–scale changes in wind. However, the direct link between this wind stress mechanism and the reinvigoration was not made by Landschützer et al. (2015). This may be, in part, due to the seasonal decoupling that may lead to biased interpretation of wind stress and SST.

We propose the link between spatial changes in wind stress and uptake of CO_2 as an alternative hypothesis to temperature being a driver as suggested by Landschützer et al. (2015). Typically an increase in ocean temperature, which reduces CO_2 solubility, results in an increase in ΔpCO_2 (Takahashi et al., 1993). However, seasonal – regional analysis shows that the observed relationship between pCO_2 and SST is counterintuitive (Figure 5a-c,g-i). On this basis we propose that SST is not a driver of pCO_2 in winter. We suggest that this relationship is a product of weaker mixing and Ekman transport that allows warmer waters to shift southward. This also has the impact of strengthening buoyancy that would otherwise bring CO_2 to the surface. In summary, our results suggest that, like pCO_2, the SST changes are also a response to the wind stress not in themselves the drivers of pCO_2 changes.

Given the hypothesis that wind stress is the dominant driver of interannual – decadal ΔpCO_2 in winter, it is of interest to understand its potential mechanisms. Past studies have used the SAM as a proxy for wind stress variability over the Southern Ocean, where the multi-decadal increasing trend has been cited as a reason for the saturation in the 1990's (Marshall, 2003; Le Quéré et al., 2007; Lenton and Matear, 2007; Lovenduski et al., 2008). While Landschützer et al. (2016) identified the SAM as being a driver of global CO_2 variability, the index does not explain the reinvigoration of the Southern Ocean CO_2 sink in the 2000s. The SAM is often represented as a zonally integrating index (Marshall, 2003), but more recent studies have shown that the SAM, as the first empirical mode of atmospheric variability, is zonally asymmetric (Fogt et al., 2012). The zonal asymmetry of the SAM is linked with ~~ENSE~~ENSO and is strongest in winter, particularly over the Pacific sector of the Southern Ocean during a positive phase, thus in accord with the Pacific–Indian winter wind stress dipole observed in Figures 5d,e (Barnes and Hartmann, 2010; Fogt et al., 2012). Fogt et al. (2012) noted that the SAM has become more zonally symmetric in summer since the 1980's, matching the wind stress anomalies seen in Figure ~~7~~6d-f.

~~DeVries et al. (2017) proposed that slowing down of Meridional Overturning Circulation (MOC) as an alternate mechanism for the reinvigoration of the Southern Ocean CO_2 sink in the 2000's. The authors explain that weaker overturning reduces the natural CO_2 brought from the deep to the surface ocean. Moreover, they suggest that this mechanism may continue to drive intensification of the global CO_2 sink. The longer modes of MOC variability makes it difficult to attribute the change in flux to changes in overturning.~~

~~This poses an interesting question for the Southern Ocean carbon sink when we consider that weakening MOC may counteract the intensification of winds over the Southern Ocean (encapsulated by the increasing SAM). Meredith et al. (2012) found that this question is made more complex by the compensatory effect of increased eddy activity (measured by eddy kinetic energy – EKE) to enhanced~~

~~northward Ekman transport driven by intensified winds (Meredith and Hogg, 2006; Abernathey et al. 2011; Marshall and Speer, 2012). Moreover, the inclusion of these eddies in a high resolution model reduced CO_2 outgassing driven by increased Ekman transport by one third by entraining alkalinity to the surface water (Dufour et al. 2013). As it stands, this is an unresolved question and more work will have to be undertaken to understand the effect of these two counteracting mechanisms of CO_2 transport.~~

In summary, we propose that interannual variability of wind stress and its regional expression in winter is the dominant interannual driver of ~~FCO_2~~ ΔpCO_2 variability in the Southern Ocean. The interannual variability of wind stress is linked to the SAM, but this relationship is nuanced by the zonally (regional) asymmetric variability of the SAM~~.~~ as observed by zonal asymmetry of wind stress in the Pacific and Indian sectors of the Southern Ocean.

3.6 ~~Trends in the anomalies~~Anomalies of ΔpCO_2 and its summer drivers ~~in summer~~

The most ~~important~~marked difference between the summer and winter anomalies, is that ΔpCO_2 (Figures 6a-c) does not correlate with wind stress (Figures ~~8d~~6d-f~~) does not correlate to ΔpCO_2 (Figures 8a-c~~), thus ruling out wind as a first order driver of summer CO_2. Rather, ΔpCO_2 has the strongest coherence with Chl-*a* (an inverse relationship), which suggests that primary production may be a first order driver of the observed ΔpCO_2 variability. Another difference between summer and winter is that the magnitudes of the transition anomalies are much larger in summer, and thus there are larger regions of significant anomalies (Figure 6a-c).

Looking more specifically at the significant variability of ΔpCO_2, ~~Transition~~transition A (P2 – P1 in Figure ~~8a~~6a) is marked by ~~patchy decreases~~ a decrease of CO_2 in ~~regions of high EKE (Agulhas retroflection and~~ the SAZ (Tasman shelf~~) in the SAZ and AZ,~~ region), mirrored by an increase in Chl-*a*. The Atlantic and Indian sectors of the PFZ remain mostly neutral/weak sources marked by a reduction in phytoplankton biomass (Figure ~~8j~~6j). Transition B (P3 – P2 in Figure ~~8b~~6b), shows invigoration of CO_2 uptake in~~:~~ the Atlantic sector of the SAZ and PFZ; ~~the Indian sector~~and in parts of the ~~AZ; and patchy strengthening in the~~ Pacific Ocean. Once again, the reduction of ΔpCO_2 ~~from P2 to P3 in the aforementioned regions correlate~~correlates well with Chl-*a* increases. In transition C (P4 – P3 in Figure ~~8c~~6c) the reduction of the ΔpCO_2 is widespread in the Indian and Pacific Oceans in all three biomes, ~~though this does not necessarily correspond with~~ as the increase in Chl-*a*~~. There~~ is ~~a strong decrease~~similarly widespread. Conversely, there is a reduction in Chl-*a* and concomitant increase in ΔpCO_2 along Polar front in the Atlantic sector, coinciding with position of the ACC, which has high EKE (Meredith, 2016). These examples demonstrate that ΔpCO_2 is driven primarily by Chl-*a* in summer. However, understanding Chl-*a* variability is ~~perhaps~~ more complex as there is seemingly no set rule between Chl-*a*, SST and wind stress (Thomalla et al~~.~~., 2011).

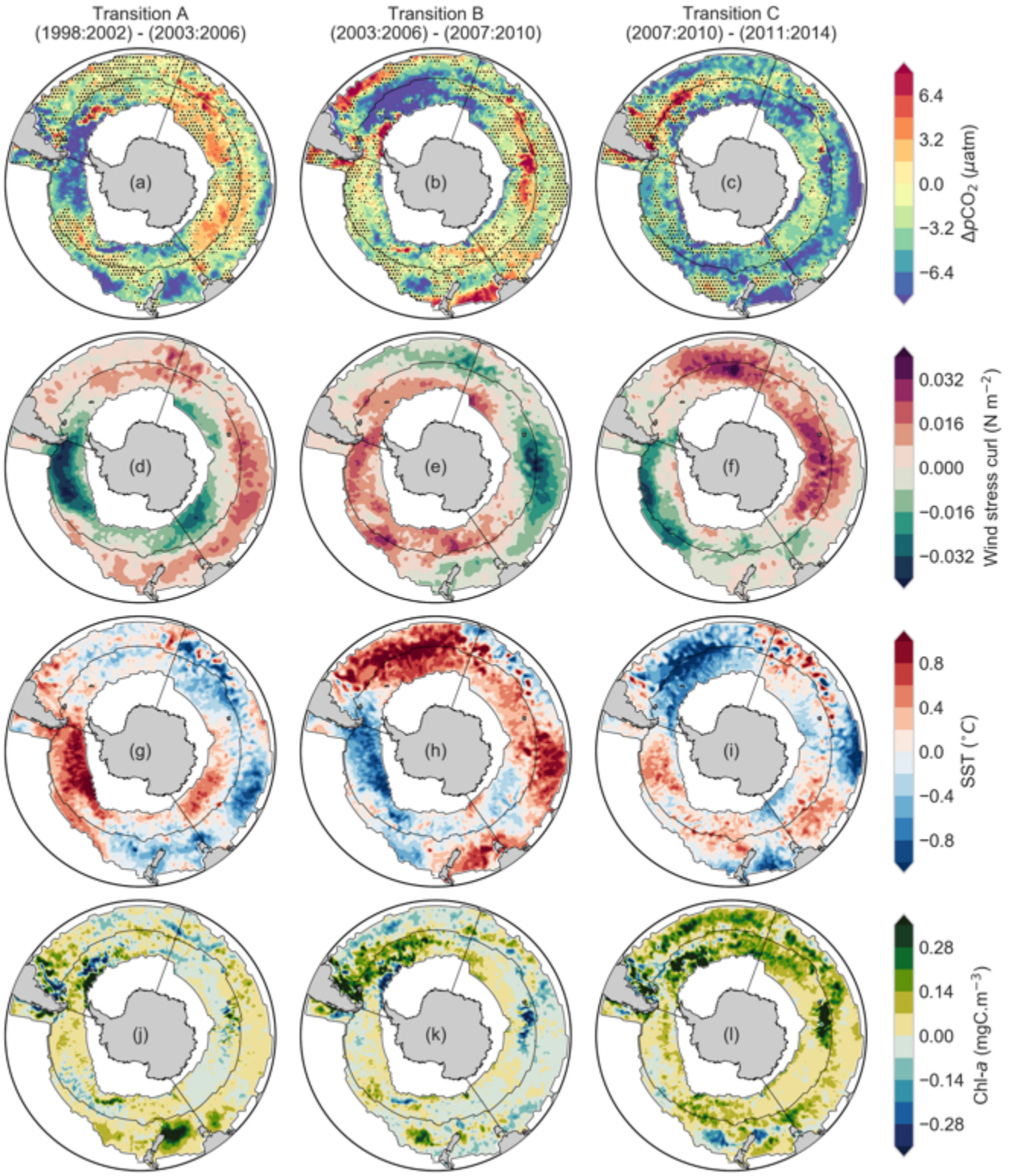

Figure ~~8: Transitions of summer ΔpCO_2, wind stress, SST and Chl-*a*~~ **]{**6: **Relative anomalies of summer ΔpCO_2 (a-c), wind stress (d-**~~e~~f**), sea surface temperature (**~~f-h~~g-i**) and mixed layer depth (**~~i-k~~j-l**) for four periods (as shown above each column). The thin black lines show the boundaries for each of the nine regions described by the biomes (Fay and McKinley**~~ 2014~~, 2014a**) and basin boundaries.**

There are regions in the Southern Ocean where summer Chl-*a* variability does not coincide with ΔpCO_2 variability, particularly in the Indian and Pacific sectors of the SAZ (Figures ~~8~~a6a-c and ~~8~~j6j-l). This may be due to ~~the fact that~~low chlorophyll concentrations, and anomalies thereof, ~~are low~~ in these regions (Thomalla et al~~.~~., 2011). ~~This may~~As a result ~~in~~ the other variables, SST and wind stress, ~~becoming~~may

be higher order drivers in low chlorophyll regions, as found by Landschützer et al. (2015) and Munro et al. (2015).

It is thus important to understand the variability of SST and wind stress in summer. Large SST anomalies between the western Atlantic and eastern Pacific sectors vary as ~~an~~a zonally asymmetric dipole. As in winter, there is a summer wind stress anomaly dipole, but rather than being zonally asymmetric (*e.g.* Pacific–Indian), the dipole has annular, north-south variability (Figures ~~7,8d~~5,6d-f). We suggest that these dipoles in the variability may indicate that the Southern Ocean, as a system, transitions between different states forced by atmospheric variability (Landschützer et al~~.~~., 2015).

~~Lastly, there~~An important note is ~~seasonal variability in~~that the magnitudes of ΔpCO_2 and ~~the~~its drivers~~.~~ ~~The~~ have different magnitudes seasonally. For example, the anomalies of ΔpCO_2 and SST ~~have a~~are larger ~~magnitude~~in summer than ~~the~~in winter ~~anomalies~~. Conversely, the wind stress anomalies are larger for winter than in summer. This is an important consideration for analyses that aim to understand the driving mechanisms, where annual averaging would make it difficult to decompose the true drivers of change.

3.6.1 Chlorophyll dominated interannual anomalies of pCO_2 in summer

~~The fact~~Our finding that Chl-*a* is the dominant driver of interannual ΔpCO_2 variability should not be surprising given that models and observations support this notion (Hoppema et al~~.~~., 1999; Bakker et al~~.~~., 2008; Mahadevan et al~~.~~., 2011; Wang et al~~.~~., 2012; Hauck et al~~.~~., 2013; 2015; Shetye et al~~.~~., 2015). However, our data show that the dominance of interannual Chl-*a* variability over ΔpCO_2 is largely limited to regions where Chl-*a* is high, such as the Atlantic, the Agulhas retroflection and south of Australia and New Zealand (Figure ~~9~~7).

~~However, the~~The spatial variability of high Chl-*a* regions in the Southern Ocean is complex due to the dynamics of light and iron limitation (Arrigo et al~~.~~., 2008; Boyd and Ellwood, 2010; Thomalla et al~~.~~., 2011; Tagliabue et al~~.~~., 2014; 2017). This complexity is highlighted in Thomalla et al. (2011), where the Chl-*a* is characterized into regions of concentration and seasonal cycle reproducibility (Figure ~~9~~7). The seasonal cycle reproducibility (SCR) is calculated as the correlation between the mean annual seasonal cycle and the observed chlorophyll time series. Here we use the approach of Thomalla et al. (2011), in Figure ~~9~~7, as a conceptual framework to understand the interannual variability of ΔpCO_2.

3.6.2 High chlorophyll regions

While regions of high SCR (dark green in Figure ~~9~~7) do not correspond with the interannual variability of Chl-*a* (Figure ~~8j~~6j-l), the framework by Thomalla et al. (2011) does present a hypothesis by which the

variability of Chl-*a* and its drivers can be interpreted. This is, that the variability of Chl-*a* in a region is a complex interaction of the response of the underlying physics (mixing vs buoyancy forcing, which modulate light (via the MLD) and iron supply, to the interannual variability in the drivers (SST and wind stress). This complexity is exemplified by strong warming in the Atlantic during transition B, which results in both an increase and decrease in Chl-*a*, with inverse consequences for ΔpCO_2. The effect is even stronger transition C, where strong cooling in the Atlantic results in both a decrease and increase of Chl-*a* (Figure 8i6i,l). In both transition A and B the respective increase and decrease of Chl-*a* occur roughly over the ACC, while the opposing effects during transitions A and B occur roughly to the north and south of the ACC region. These temperature changes may impact the stratification of the region, but complex interaction with the underlying physics results in variable changes in Chl-*a*.

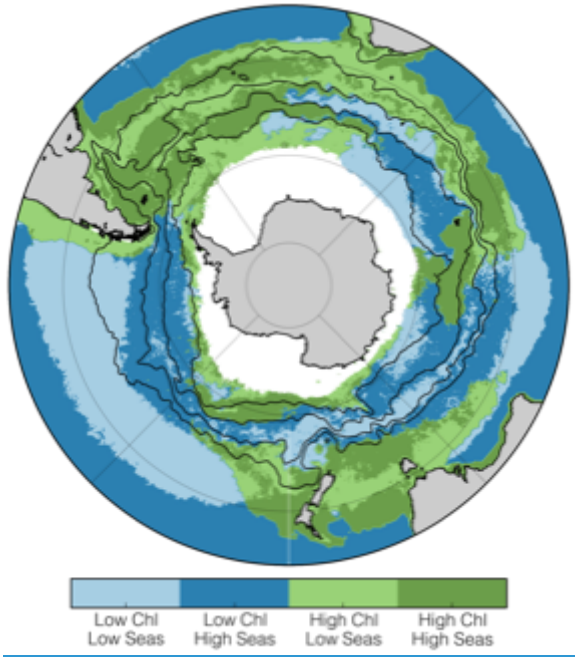

Figure 9: Chl-*a* seasonal cycle reproducibility and iron supply mechanisms in the Southern Ocean]{(a) Regions of chlorophyll biomass and seasonal cycle reproducibility from Thomalla et al. (2011) (using SeaWIFS data). Seasonality is calculated as the correlation between the mean annual seasonal cycle compared to the observed chlorophyll time series. A correlation threshold of 0.4 was applied to each time series to distinguish between regions of high and low seasonality; similarly, a threshold of 0.25 mg m^{-3} was used to distinguish between low or high chlorophyll waters. Black lines showing the fronts are the same as described in figure.

It is clear that, while there is a relationship between Chl-*a* and pCO_2 as well as a relationship between wind stress and SST in summer, the relationship between wind forcing and, Chl-*a* and pCO_2 is not as strong as in the winter anomalies (Figure 7). The reason for this is likely to5). It may be that enhanced summer buoyancy forcing resulting from summer warming and mixed layer eddies drives a more complex response to wind stress in the form of vertical velocities (w) and mixing (Kz),, which influence the iron supply and the depth of mixing depth (McGillicuddy, 2016; Mahadevan et al., 2012).

Mesoscale and sub-mesoscale processes may have a part to play in these dynamic responses of Chl-*a* to changes in SST and wind stress (amongst other drivers). For example, eddy-driven slumping is a sub-

~~mesoscale process that acts~~could act to rapidly shoal the mixed layer (Mahadevan et al~~.~~., 2012; Swart et al., 2015b; du Plessis et al., 2017). This allows phytoplankton to remain within the euphotic zone and thus grow (while iron is not limiting). Similarly, Nicholson et al. (2016) and Whitt et al. (2017) demonstrated that ~~a combination of high and low frequency oscillation of down-front winds are able to enhance nutrient entrainment (including~~submesoscale processes could supply iron~~) into~~ to the mixed layer ~~on the less dense side of a front. This has important implications for Southern Ocean fronts, where Chl-*a* may benefit from this entrainment mechanism combined with eddy-driven slumping that could subsequently rapidly shoal the mixed layer (Du Plessis et al.~~by submesoscale ~~2017).~~

~~Storm driven, intra-seasonal~~ mixing ~~is another sub-mesoscale process that could alleviate iron limitation through shear-driven mixing along the base of the mixed layer (Nicholson et al. 2016).~~. Importantly, ~~both storm-driven entrainment and the oscillatory enhancement of entrainment,~~these mechanisms rely on a mixing transition layer that has sufficient iron that is able to sustain growth – weak dissolved iron gradients in the Pacific and east Indian sectors of the Southern Ocean ~~would~~could explain the lack of phytoplankton in these regions (Tagliabue et al~~.~~., 2014; Nicholson et al~~.~~., 2016). Much of the spatial character of the transition anomalies occurs at mesoscale, which strengthens the view that these mesoscale and sub-mesoscale processes may be key to explain changes in Chl-*a* (Figure ~~8j-l). This level of mechanistic detail was not part of this study.~~6j-l).

3.6.3 Low chlorophyll regions

Entrainment and stratification can explain much of the variability in the eastern Pacific and Indian sector of the PFZ (with the exception of the wake of the Kerguelen Plateau). For example, in the eastern Pacific in transition A (Figure ~~8a~~6a,d,g), strong warming and weaker winds have little impact on Chl-*a*, but a decrease in ΔpCO_2 is observed. Conversely, cooling in the west Indian sector of the PFZ results in a weak increase in ΔpCO_2 during the same transition. In both these cases, the effect of cooling or warming on ΔpCO_2 is negligible relative to the impact of entrainment or stratification respectively. The effect is reversed in the eastern Pacific during transition B where strong cooling results in a weak reduction of ΔpCO_2 rather than the increase that would be expected from entrainment. This is the mechanism that Landschützer et al. ~~(2015) describe in the Pacific, where enhanced entrainment of DIC and TA is compensated for by cooling. This emphasises that the balance between SST (as a driver of stratification) and wind stress is far more important than in winter~~(2015) ascribed to the reduction of ΔpCO_2 in the Pacific, but the effect observed in 6b is weak.

In summary, regions with high biomass~~,~~ Chl-*a* integrates the complex interactions between SST, wind stress, MLD and sub-mesoscale variability resulting in large interannual pCO_2 variability compared to

low biomass regions. In low Chl-*a* regions, wind driven entrainment/stratification are ~~in general dominant over thermally driven changes~~more likely drivers of ΔpCO_2.

4 Synthesis

In this study, an ensemble ~~means~~mean of empirically estimated ΔpCO_2 ~~and FCO_2 were~~is used to investigate the trends and the drivers of these trends in the Southern Ocean. The ~~ensemble mean of~~estimated ΔpCO_2 ~~showed~~shows that the seasonal cycle is the dominant mode of variability imposed upon ~~a~~ weaker interannual ~~and decadal trends.~~variability. The data ~~were~~are separated into ~~nine~~ domains defined by functional biomes and oceanic basins to account for the roughly basin scale zonal asymmetry observed in preliminary analyses of ΔpCO_2 (Fay and McKinley, ~~2014~~2014a). A seasonal decomposition ~~was~~is applied to the ~~nine~~ domains, revealing that winter and summer ~~interannual trends are~~variability is decoupled for each region. ~~The decadal trend was~~increase and subsequent decrease of pCO_2 (and air-sea CO_2 fluxes) is in accordance with recent studies showing a saturation of the Southern Ocean CO_2 sink in the 1990's followed by the reinvigoration in the 2000's (Le Quéré et al~~.~~., 2007; Landschützer et al~~.~~., 2015).

We suggest that changes in the characteristics of the seasonal cycle of the drivers of pCO_2 define the interannual ~~and decadal modes. The~~ variability pCO_2. In other words, the mechanisms that drive ~~the~~ interannual ~~and decadal~~ modes of variability are ~~therefore~~ embedded in the seasonal cycle.

We propose that winter ΔpCO_2 ~~decadal~~ variability is driven ~~by~~ primarily by changes in ~~the~~ winter wind stress, which influences the resulting convective entrainment of deep DIC-rich water masses (Lenton et al~~.~~., 2009; 2013). This winter variability has a longer mode than summer inter-annual variability. We attribute this longer winter mode of variability to the Southern Annular Mode, which has a decadal mode (Lovenduski et al., 2008; Fogt et al., 2012; Landschützer et al., 2016). This mechanism is ~~strongest~~likely dominant in winter due to ~~the~~its role ~~of~~in large seasonal net heat losses ~~on~~that drive convective overturning of the water column. ~~The ΔpCO_2 winter trends, agreed with wind stress variability, where the latter corresponds with the decadal variability associated with the Southern Annular Mode (Lovenduski et al. 2008; Fogt et al. 2012; Landschützer et al. 2016).~~

~~Our findings show~~We suggest that interannual summer variability of ΔpCO_2 occurs from a baseline set by an interannual winter trend ~~but~~. Moreover, the shorter time-scale summer ~~linked~~ interannual variability of ΔpCO_2 (roughly 4 – 6 years) ~~was~~is driven primarily by Chl-*a*. Wind stress and sea surface temperature still ~~influenced~~influence ΔpCO_2 in summer, but ~~were~~are lower order drivers. We propose that the

interannual variability of the summer seasonal peak is linked to the complex interaction of mid-latitude storms with the strong mesoscale and sub-mesoscale gradients in the Southern Ocean.

~~We~~Overall, we propose that ~~there needs to be a more concerted focus through in situ and modelling experiment towards understanding~~ although the winter wind-stress linked mechanisms ~~that drive seasonal and intraseasonal variability in order to improve~~ explain the ~~ability of ocean and earth systems models in reflecting and predicting~~ decadal ~~and interannual modes.~~

A Additional Materials

A1 Mean ΔpCO_2 for Southern Ocean domains

The SAZ (Figures 5a-c) accounts for trends in the majority of strengthening and weakening of CO_2 uptake in the Southern Ocean with a mean ΔpCO_2 of -25.31 µatm. However, there is a relatively large difference between the three sectors of the SAZ, with mean ΔpCO_2 values of -24.39, -22.24 and -30.48 µatm for the Indian, Pacific and Atlantic respectively. In the PFZ (Figures 5d-f) the sink is far weaker due to the opposing summer uptake and winter outgassing, with ΔpCO_2 values of 0.23, -2.06 and -6.57 again in the respective order Indian, Pacific and Atlantic. Similarly, in the AZ (Figures 5g-i) mean estimates of ΔpCO_2 are muted by opposing seasonal signals with mean estimates of 4.83, -3.01 and -0.76 µatm.by the Southern Ocean, summer drivers may explain the inter-annual variability in the decadal trends (Lovenduski et al., 2008; Landschützer et al., 2015).

Lastly the ensemble of machine learning methods shows that there is still considerable disagreement between the different approaches. This is likely driven by the lack of pCO_2 measurements in the Southern Ocean as found by Rödenbeck et al. (2015). *Table 2: Mean $\Delta pCO2$ for each of the Southern Ocean domains shown in Figure 5, where the domains are defined according to Figure 1.*

BIOME	Indian	Pacific	Atlantic
SAZ	-24.39	-22.25	-30.48
PFZ	0.23	-2.06	-6.57
AZ	4.83	-3.01	-0.76

A2Autonomous sampling platforms will likely play a role in closing this "observation gap", but strategic deployment and sampling strategies will be critical to constrain and improve our understanding of CO_2 in the non-stationary context (McNeil and Matear, 2013; Monteiro et al., 2015).

S Supplementary Materials

S1 Wind speed and regional surface area

The regional magnitude of integrated air-sea CO_2 fluxes are in part determined by the wind speed and surface area of the specific region. Figure ~~1a~~S1a shows the average wind speeds for summer and winter for each of the regions as defined in Figure 1. The wind product used is CCMP v2 (Atlas et al. 2011). Figure ~~1b~~S1b shows the surface area of each of the regions. Note that the Indian sector of the PFZ has both the highest average wind speed and has the largest surface area. This explains the dominance of the region in the determination of interannual ~~trends~~variability of FCO_2~~,~~ (Figure S2), even though ΔpCO_2 ~~trends~~(Figure 4) variability are relatively weak.

Figure ~~A1~~S1: (a) Average wind speeds for each of the ~~bimoes~~biomes for summer (dark) and winter (light). The ocean basins are shown by the ~~colors~~colours as shown in the key for (b). (b) shows the size of each region ~~seperated~~separated by biome and basin.

~~**A3 Additional transition anomaly figures**~~

~~Figure A2 and A3 augment Figures 7 and 8 respectively. These were omitted from the main text figures as we found that these variables (Chl-*a* in winter and MLD in summer) do little to aid our understanding of changes in ΔpCO_2. These are included for the sake of completeness.~~

~~*Figure A2: Winter Chl-a transitions for each of the three anomaly periods (relating to Figure 7).*~~

~~**Figure A3: Summer MLD transitions**~~

S2 Seasonal time series

Figure S2: The regional breakdown of the seasonal averages for ΔpCO_2. The seasonal mean for summer (solid) and winter (dashed) for each method is represented by the different coloured lines as shown in the key, where MLS is the Mixed Layer Scheme. The other methods are as in the main text. The grey fill is the ensemble mean $\Delta pCO_2 \pm E_b$ where E_b is the between-method error calculated as in Eq (5).

Figure S2 shows the seasonal time series for each ~~of the three anomaly periods (relating to Figure 8).~~region maintaining separate seasonal averages for each method. We also include the Marginal Ice Zone plots with all plots showing the average between-method error.

The Mixed Layer Scheme (MLS) method by Rödenbeck et al. (2013) is also included. Note that the ~~scale of MLD~~MLS is not a machine learning method as it incorporates prior knowledge of the system. The method results in divergent estimates of ΔpCO_2, particularly in the SAZ. The MLS fails to produce a seasonal cycle with winter and summer ΔpCO_2 having the same magnitude. Further work will have to be done to understand the cause for this difference. We do not include MLS in the main ensemble as we cannot explain this difference. The methods are in much better agreement in the PFZ and MIZ.

S3 Air-Sea CO_2 Fluxes

Air sea CO_2 fluxes are calculated with:

$$FCO_2 = k_w \cdot K_0 \cdot (pCO_2^{sea} - pCO_2^{atm}) \quad (S1)$$

The gas transfer velocity (k_w) is calculated using a quadratic dependency of wind speed with the coefficients of (Wanninkhof et al., 2009). Coefficients from Weiss (1974) are used to calculate K_0 and ΔpCO_2 is estimated by the empirical models. ~~figure~~Wind speed is calculated from the u and v vectors ($\sqrt{u^2 + v^2}$) of the Cross-Calibrated Multiplatform Product (CCMP) v2 (Atlas et al., 2011; Wentz et al., 2015). Wind speed is one of the largest contributors to the uncertainty in flux estimates, thus the choice of the wind product could have a large impact on flux estimates as well as interpretation of the drivers of CO_2 (Takahashi et al., 2009). We use the ensemble mean ΔpCO_2 from Figure 4 to calculate fluxes - note that this does not ~~match~~include the ~~scale of MLD~~MLS shown in Figure S2.

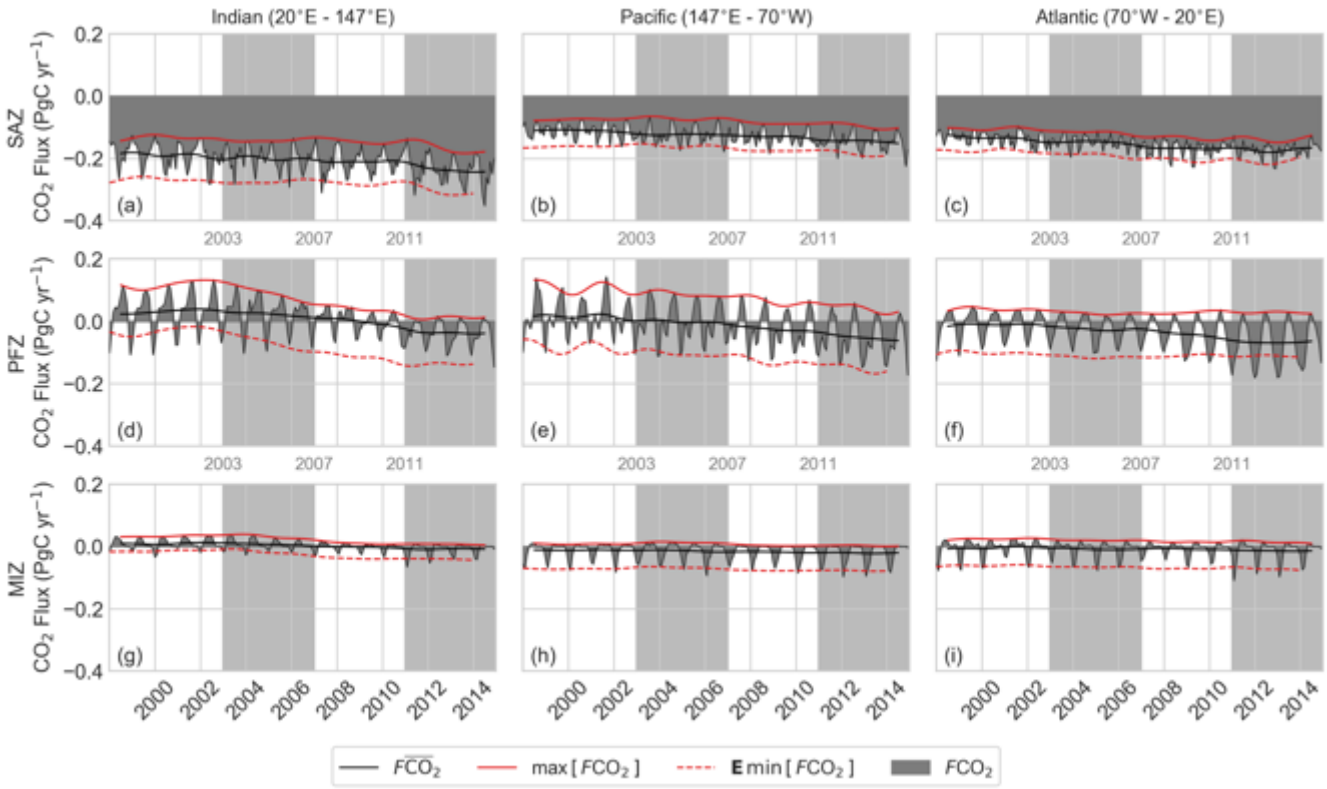

Figure S3: FCO_2 (dark grey) plotted by biome (rows) and basin (columns). Biomes are defined by Fay and McKinley (2014a). The solid red line shows the maximum for each year (winter outgassing) and the dashed line shows the same line less the average difference between the minimum and maximum – this is the expected amplitude. Lighter grey shading in (a-i) shows periods used in Figure ~~7.~~ 5 and 6. Note that fluxes in the MIZ are calculated from a reduces surface area to maintain consistency between methods.

Mean FCO_2 is shown in Figure S3. Note that the apparent weak fluxes in the MIZ are due to the reduction of the surface area and thus flux to maintain equal weighting between machine learning methods. The SAZ clearly dominates the annual uptake of CO_2 in the Southern Ocean, but the interannual variability is dominated by the PFZ. An interesting point of the SAZ is that the seasonal cycle of wind speed (strong in winter, weak in summer) opposes that of ΔpCO_2 sink (weak in winter, strong in summer). The net result is that, compared to ΔpCO_2, the seasonal amplitude of FCO_2 is reduced. The same effect shifts the

mean flux in the PFZ, but does not affect the amplitude, where outgassing is amplified in winter and the sink is weaker than if wind speed was constant. Lastly, Figures S3a,d show that the Indian sector of the Southern Ocean dominate both uptake (SAZ) and the interannual variability (PFZ).

S4 Uncertainty of the transition anomalies

The transition anomalies are not calculated from the mean of the three methods. Rather we calculate the anomalies for each individual method with:

$$a_{n(p')} = \overline{s_n}_{(p)} - \overline{s_n}_{(p-1)} \quad \text{(S2)}$$

where *s* are the estimates for a particular model, *n* represents an individual model and *p* represents P1 to P4. The result, $a_{n(p')}$ thus represents the anomaly for two periods for a particular model. We then calculate the average of the anomalies with:

$$a_{p'} = \frac{1}{N} \cdot \sum_{n=1}^{N} a_{n(p')} \quad \text{(S3)}$$

where *N* is 3, the number of models. We then calculate the standard deviation of the three anomalies ($e_{p'}$), which is analogous to the between-model error, with:

$$e_{p'} = \sqrt{\frac{1}{N} \cdot \sum_{n=1}^{N} (a_{n(p')} - \overline{a_{n(p')}})^2} \quad \text{(S4)}$$

where the terms are consistent with those above. We use $e_{p'}$ as an uncertainty threshold where anomalies are only considered significant if $|a_{p'}| > e_{p'}$. These regions are masked in Figures 5a-c and 6a-c. Figure S4 shows the winter (a-c) and summer (d-f) $e_{p'}$ for each transition anomaly.

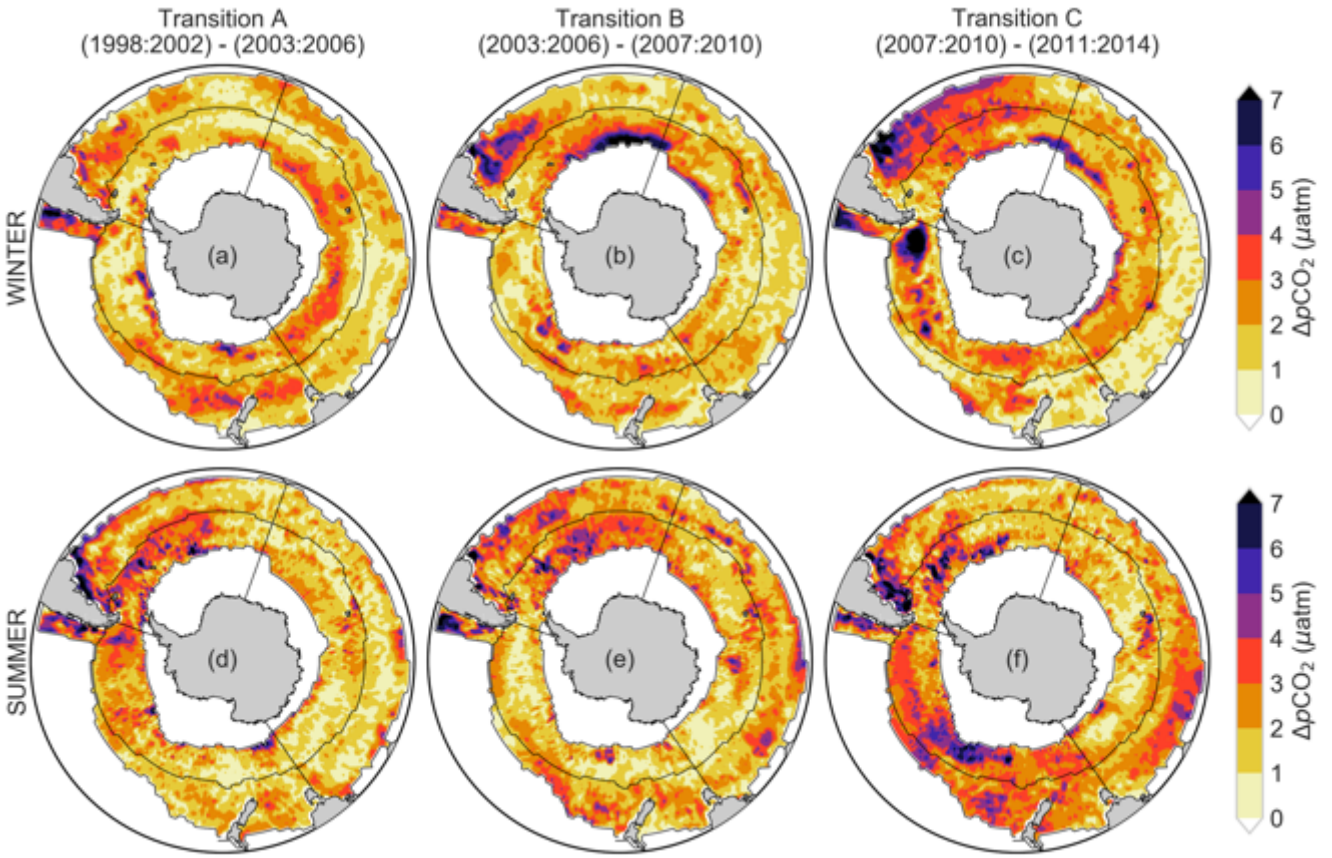

Figure S4: Maps of the standard deviation between empirical methods for the anomalies. These are used as thresholds for ΔpCO_2 in Figures 5(a-c) and 6(a-c) for winter and summer respectively. When the standard deviation exceeds the absolute value average anomaly, the values are masked as shown in Figures 5 and 6.

S5 Additional driver variables

Here we show additional variables that accompany Figures 5 and 6. Figure S5 shows winter Chl-*a*, u- and v-components of wind and Figure S6 shows summer MLD, u- and v-components of wind. These variables were not included in the main analyses as they did not contribute significant information to the proxy variables already present (wind stress, SST and MLD/Chl-*a*). It is interesting to note that the u- and v- components of wind speed highlight the zonally asymmetric dipole during winter (Figures S5d,e,g,h) and the annular dipole during summer (Figures S6d,e).

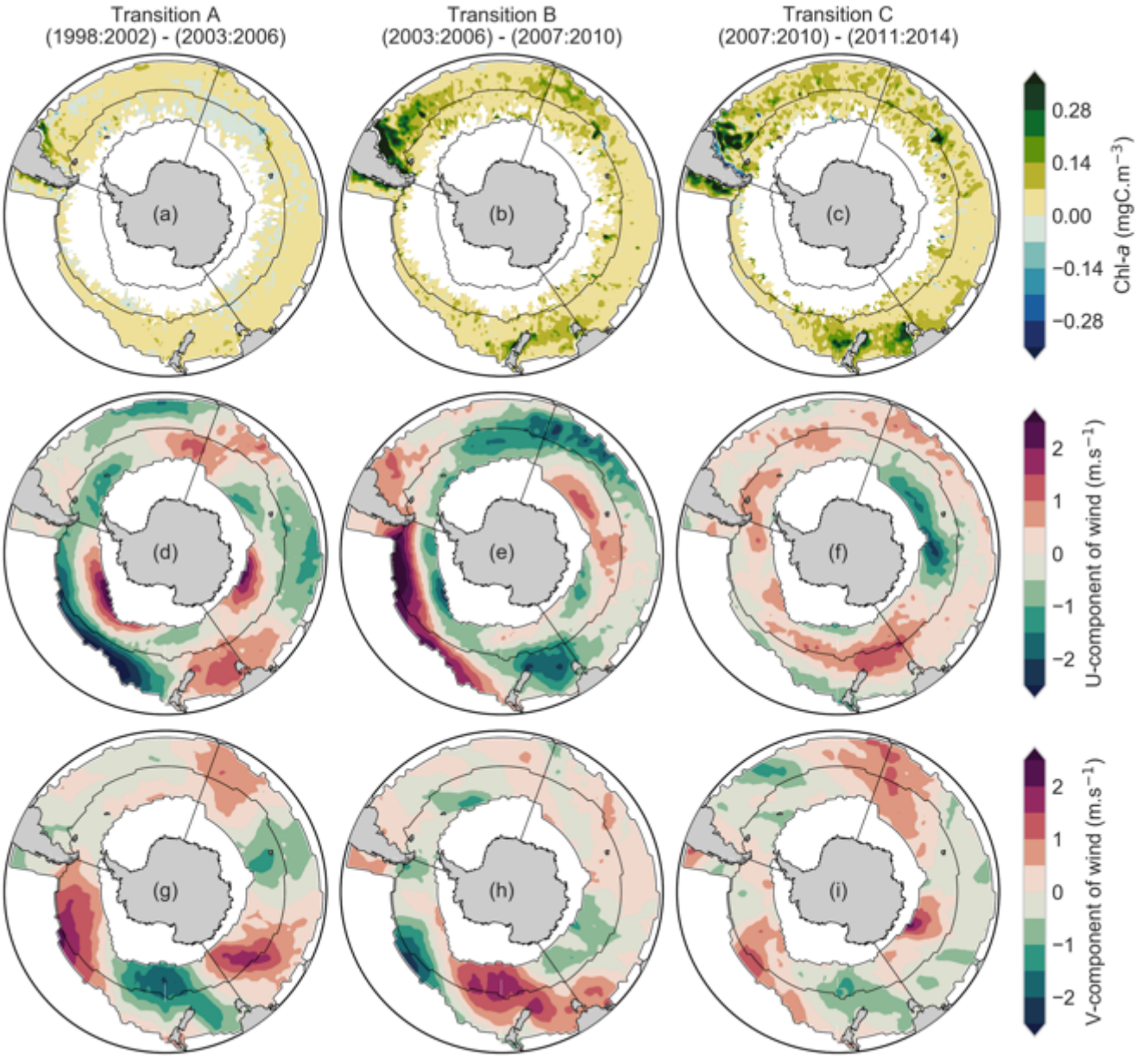

Figure S5: Relative anomalies of winter chlorophyll-a (a-c), u- (d-f), and v-components (g-i) of wind for four periods (as shown above each column). The thin black lines show the boundaries for each of the nine regions described by the biomes (Fay and McKinley, 2014a) and basin boundaries.

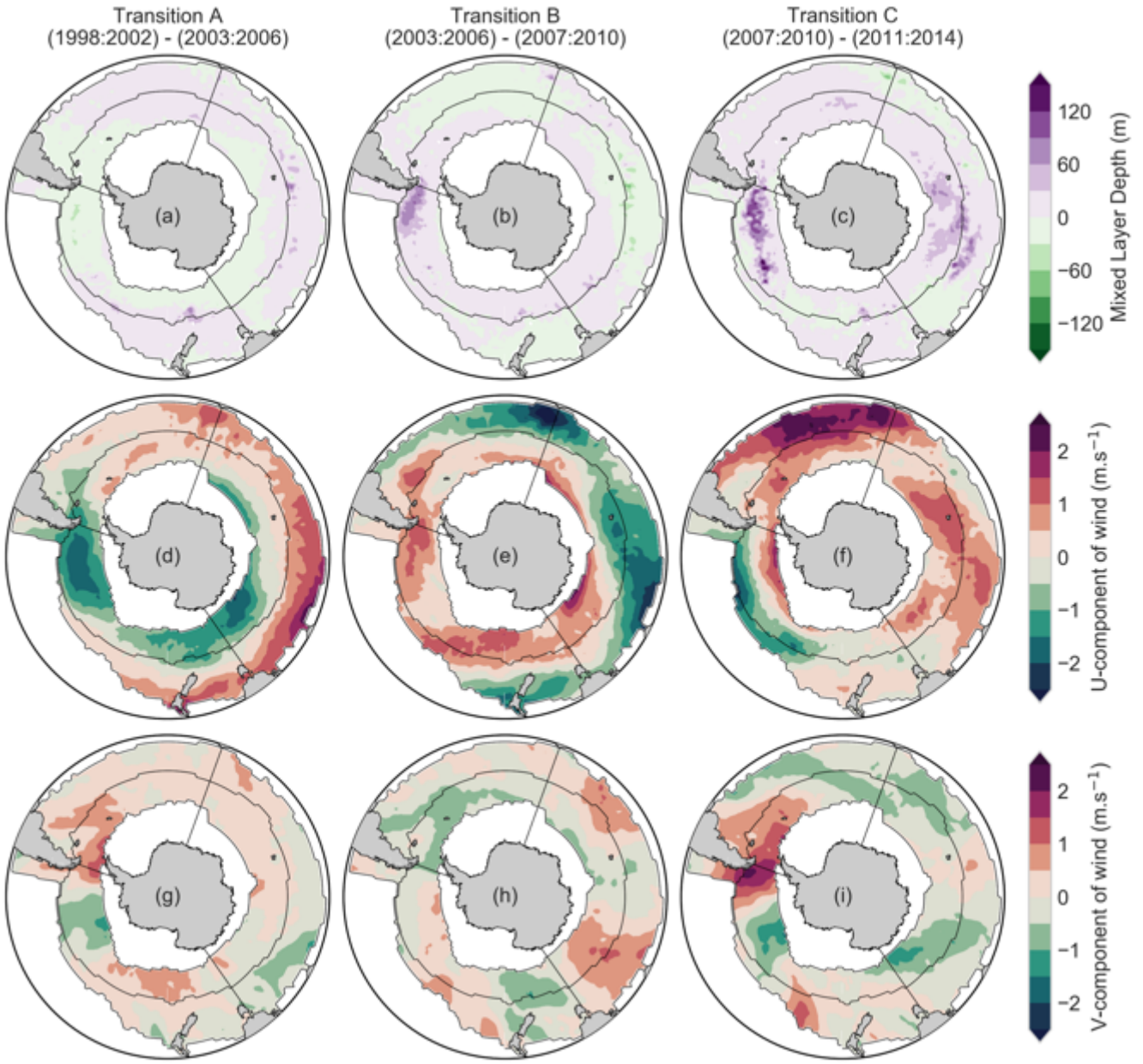

Figure S6: Relative anomalies of summer mixed layer depth (a-c), u- (d-f), and v-components (g-i) of wind for four periods (as shown above each column).. The thin black lines show the boundaries for each of the nine regions described by the biomes (Fay and McKinley, 2014a) and basin boundaries.

References

Abernathey, R., Marshall, J. C., & Ferreira, D. (2011). The Dependence of Southern Ocean Meridional Overturning on Wind Stress. *Journal of Physical Oceanography*, *41*(12), 2261–2278. https://doi.org/10.1175/JPO-D-11-023.1

Arrigo, K. R., van Dijken, G. L., & Bushinsky, S. (2008). Primary production in the Southern Ocean, 1997-2006. *Journal of Geophysical Research*, *113*(8), 1997–2006. https://doi.org/10.1029/2007JC004551

Atlas, R., Hoffman, R. N., Ardizzone, J., Leidner, S. M., Jusem, J. C., Smith, D. K., & Gombos, D. (2011). A Cross-calibrated, Multiplatform Ocean Surface Wind Velocity Product for Meteorological and Oceanographic Applications. *Bulletin of the American Meteorological Society*, *92*(2), 157–174. https://doi.org/10.1175/2010BAMS2946.1

Bakker, D. C. E., Hoppema, M., Schr, M., Geibert, W., & Baar, H. J. W. De. (2008). A rapid transition from ice covered CO2-rich waters to a biologically mediated CO2 sink in the eastern Weddell Gyre. *Biogeosciences*, *5*, 1373–1386.

Bakker, D. C. E., Pfeil, B., Landa, C. S., Metzl, N., O'Brien, K. M., Olsen, A., … Xu, S. (2016). A multi-decade record of high-quality fCO2 data in version 3 of the Surface Ocean CO2 Atlas (SOCAT). *Earth System Science Data*, *8*(2), 383–413. https://doi.org/10.5194/essd-8-383-2016

Bakker, D. C. E., Pfeil, B., Smith, K., Hankin, S., Olsen, A., Alin, S. R., … Watson, A. J. (2014). An update to the surface ocean CO2 atlas (SOCAT version 2). *Earth System Science Data*, *6*(1), 69–90. https://doi.org/10.5194/essd-6-69-2014

Barnes, E. A., & Hartmann, D. L. (2010). Dynamical Feedbacks of the Southern Annular Mode in Winter and Summer. *Journal of the Atmospheric Sciences*, *67*(2007), 2320–2330. https://doi.org/10.1175/2010JAS3385.1

Boyd, P. W., & Ellwood, M. J. (2010). The biogeochemical cycle of iron in the ocean. *Nature Geoscience*, *3*(10), 675–682. https://doi.org/10.1038/ngeo964

Butterworth, B. J., & Miller, S. D. (2016). Air-sea exchange of carbon dioxide in the Southern Ocean and Antarctic marginal ice zone. *Geophysical Research Letters*, *43*(13), 7223–7230. https://doi.org/10.1002/2016GL069581

Carranza, M. M., & Gille, S. T. (2015). Southern Ocean wind-driven entrainment enhances satellite chlorophyll-a through the summer. *Journal of Geophysical Research: Oceans*, *120*(1), 304–323. https://doi.org/10.1002/2014JC010203

CDIAC. (2017). *Multi-laboratory compilation of atmospheric carbon dioxide data for the period 1957-2016*. NOAA Earth System Research Laboratory, Global Monitoring Division. https://doi.org/10.15138/G3CW4Q

Chierici, M., Signorini, S. R., Mattsdotter-Björk, M., Fransson, A., & Olsen, A. (2012). Surface water fCO 2 algorithms for the high-latitude Pacific sector of the Southern Ocean. *Remote Sensing of Environment*, *119*, 184–196. https://doi.org/10.1016/j.rse.2011.12.020

de Boyer Montégut, C., Madec, G., Fischer, A. S., Lazar, A., & Iudicone, D. (2004). Mixed layer depth over the global ocean: An examination of profile data and a profile-based climatology. *Journal of Geophysical Research*, *109*(12), 1–20. https://doi.org/10.1029/2004JC002378

DeVries, T., Holzer, M., & Primeau, F. (2017). Recent increase in oceanic carbon uptake driven by weaker upper-ocean overturning. *Nature*, *542*(7640), 215–218. https://doi.org/10.1038/nature21068

Dufour, C. O., Sommer, J. Le, Gehlen, M., Orr, J. C., Molines, J.-M., Simeon, J., & Barnier, B. (2013). Eddy compensation and controls of the enhanced sea-to-air CO2 flux during positive phases of the Southern Annular Mode. *Global Biogeochemical Cycles*, *27*(3), 950–961. https://doi.org/10.1002/gbc.20090

Fay, A. R., & McKinley, G. A. (2014). Global open-ocean biomes: Mean and temporal variability. *Earth System Science Data*, *6*(2), 273–284. https://doi.org/10.5194/essd-6-273-2014

Fay, A. R., & McKinley, G. A. (2017). Correlations of surface ocean pCO2 to satellite chlorophyll on monthly to interannual timescales. *Global Biogeochemical Cycles*, *31*(3), 1–20. https://doi.org/10.1002/2016GB005563

Fay, A. R., McKinley, G. A., & Lovenduski, N. S. (2014). Southern Ocean carbon trends: Sensitivity to methods. *Geophysical Research Letters*, *41*(19), 6833–6840. https://doi.org/10.1002/2014GL061324

Fogt, R. L., Jones, J. M., & Renwick, J. (2012). Seasonal zonal asymmetries in the southern annular mode and their impact on regional temperature anomalies. *Journal of Climate*, *25*(18), 6253–6270. https://doi.org/10.1175/JCLI-D-11-00474.1

Gade, K. (2010). A Non-singular Horizontal Position Representation. *Journal of Navigation*, *63*(3), 395–417. https://doi.org/10.1017/S0373463309990415

Gregor, L., Kok, S., & Monteiro, P. M. S. (2017). Empirical methods for the estimation of Southern Ocean CO2: Support Vectorsupport vector and Random Forest Regression.random forest regression. *Biogeosciences Discussions*, (June), 1–18., *14*(23), 5551–5569. https://doi.org/10.5194/bg-14-5551-2017-215

Gurney, K. R., Law, R. M., Denning, A. S., Rayner, P. J., Pak, B. C., Baker, D., … Taguchi, S. (2004). Transcom 3 inversion intercomparison: Model mean results for the estimation of seasonal carbon sources and sinks. *Global Biogeochemical Cycles*, *18*(1), n/a-n/a. https://doi.org/10.1029/2003GB002111

Hauck, J., Völker, C., Wang, T., Hoppema, M., Losch, M., & Wolf-Gladrow, D. A. (2013). Seasonally different carbon flux changes in the Southern Ocean in response to the southern annular mode. *Global Biogeochemical Cycles*, *27*(4), 1236–1245. https://doi.org/10.1002/2013GB004600

Hoppema, M., Fahrbach, E., Stoll, M. H. C., & de Baar, H. J. W. (1999). Annual uptake of atmospheric CO2 by the Weddell sea derived from a surface layer balance, including estimations of entrainment and new production. *Journal of Marine Systems*, *19*(4), 219–233. https://doi.org/10.1016/S0924-7963(98)00091-8

Ishii, M., Inoue, H. Y., Matsueda, H., & Tanoue, E. (1998). Close coupling between seasonal biological production and dynamics of dissolved inorganic carbon in the Indian Ocean sector and the western Pacific Ocean sector of the Antarctic Ocean. *Deep-Sea Research Part I: Oceanographic Research Papers*, *45*(7), 1187–1209. https://doi.org/10.1016/S0967-0637(98)00010-7

Jones, S. D., Le Quéré, C., & Rdenbeck, C. (2012). Autocorrelation characteristics of surface ocean pCO2 and air-sea CO2 fluxes. *Global Biogeochemical Cycles*, *26*(2), 1–12. https://doi.org/10.1029/2010GB004017

Kanamitsu, M., Ebisuzaki, W., Woollen, J., Yang, S. K., Hnilo, J. J., Fiorino, M., & Potter, G. L. (2002). NCEP-DOE AMIP-II reanalysis (R-2). *Bulletin of the American Meteorological Society*, *83*(11), 1631–1643+1559. https://doi.org/10.1175/BAMS-83-11-1631

Khatiwala, S., Tanhua, T., Mikaloff Fletcher, S. E., Gerber, M., Doney, S. C., Graven, H. D., … Sabine, C. L. (2013). Global ocean storage of anthropogenic carbon. *Biogeosciences*, *10*(4), 2169–2191. https://doi.org/10.5194/bg-10-2169-2013

Landschützer, P., Gruber, N., & Bakker, D. C. E. (2016). Decadal variations and trends of the global ocean carbon sink. *Global Biogeochemical Cycles*, *30*(10), 1396–1417. https://doi.org/10.1002/2015GB005359

Landschützer, P., Gruber, N., & Bakker, D. C. E. (2017). An updated observation-based global monthly gridded sea surface pCO2 and air-sea CO2 flux product from 1982 through 2015 and its monthly climatology (NCEI Accession 0160558) Version 2.2.

Landschützer, P., Gruber, N., Bakker, D. C. E., & Schuster, U. (2014). Recent variability of the global ocean carbon sink. *Global and Planetary Change*, 927–949. https://doi.org/10.1002/2014GB004853.Received

Landschützer, P., Gruber, N., Haumann, F. A., Rödenbeck, C., Bakker, D. C. E., Van Heuven, S. M. A. C., … Wanninkhof, R. H. (2015). The reinvigoration of the Southern Ocean carbon sink. *Science*, *349*(6253), 1221–1224. https://doi.org/10.1126/science.aab2620

Le Quéré, C., Rödenbeck, C., Buitenhuis, E. T., Conway, T. J., Langenfelds, R., Gomez, A., … Heimann, M. (2007). Saturation of the Southern Ocean CO2 Sink Due to Recent Climate Change. *Science*, *316*(5832), 1735–1738. https://doi.org/10.1126/science.1137004

Lenton, A., Codron, F., Bopp, L., Metzl, N., Cadule, P., Tagliabue, A., & Le Sommer, J. (2009). Stratospheric ozone depletion reduces ocean carbon uptake and enhances ocean acidification. *Geophysical Research Letters*, *36*(12), 1–5. https://doi.org/10.1029/2009GL038227

Lenton, A., & Matear, R. J. (2007). Role of the Southern Annular Mode (SAM) in Southern Ocean CO2 uptake. *Global Biogeochemical Cycles*, *21*(2), 1–17. https://doi.org/10.1029/2006GB002714

Lenton, A., Metzl, N., Takahashi, T. T., Kuchinke, M., Matear, R. J., Roy, T., … Tilbrook, B. (2012). The observed evolution of oceanic pCO2 and its drivers over the last two decades. *Global Biogeochemical Cycles*, *26*(2), 1–14. https://doi.org/10.1029/2011GB004095

Lenton, A., Tilbrook, B., Law, R. M., Bakker, D. C. E., Doney, S. C., Gruber, N., … Takahashi, T. T. (2013). Sea-air CO2 fluxes in the Southern Ocean for the period 1990-2009. *Biogeosciences*, *10*(6), 4037–4054. https://doi.org/10.5194/bg-10-4037-2013

Lévy, M., Iovino, D., Resplandy, L., Klein, P., Madec, G., Tréguier, A. M., … Takahashi, K. (2012). Large-scale impacts of submesoscale dynamics on phytoplankton: Local and remote effects. *Ocean Modelling*, *43–44*, 77–93. https://doi.org/10.1016/j.ocemod.2011.12.003

Lovenduski, N. S., Gruber, N., & Doney, S. C. (2008). Toward a mechanistic understanding of the decadal trends in the Southern Ocean carbon sink. *Global Biogeochemical Cycles*, *22*(3), 9. https://doi.org/10.1029/2007GB003139

Lovenduski, N. S., Gruber, N., Doney, S. C., & Lima, I. D. (2007). Enhanced CO2 outgassing in the Southern Ocean from a positive phase of the Southern Annular Mode. *Global Biogeochemical Cycles*, *21*(2), 1–14. https://doi.org/10.1029/2006GB002900

Mahadevan, A., D'Asaro, E., Lee, C., & Perry, M. J. (2012). Eddy-Driven Stratification Initiates North Atlantic Spring Phytoplankton Blooms. *Science*, *337*(6090), 54–58. https://doi.org/10.1126/science.1218740

Mahadevan, A., Tagliabue, A., Bopp, L., Lenton, A., Mémery, L., & Lévy, M. (2011). Impact of episodic vertical fluxes on sea surface pCO2. *Philosophical Transactions of the Royal Society*, *369*(1943), 2009–2025. https://doi.org/10.1098/rsta.2010.0340

Maritorena, S., & Siegel, D. A. (2005). Consistent merging of satellite ocean color data sets using a bio-optical model. *Remote Sensing of Environment*, *94*(4), 429–440. https://doi.org/10.1016/j.rse.2004.08.014

Marshall, G. J. (2003). Trends in the Southern Annular Mode from observations and reanalyses. *Journal of Climate*, *16*(24), 4134–4143. https://doi.org/10.1175/1520-0442(2003)016<4134:TITSAM>2.0.CO;2

Marshall, J. C., & Speer, K. (2012). Closure of the meridional overturning circulation through Southern Ocean upwelling. *Nature Geoscience*, *5*(3), 171–180. https://doi.org/10.1038/ngeo1391

McGillicuddy, D. J. (2016). *Mechanisms of Physical-Biological-Biogeochemical Interaction at the Oceanic Mesoscale*. *Annual Review of Marine Science* (Vol. 8). https://doi.org/10.1146/annurev-marine-010814-015606

McNeil, B. I., & Matear, R. J. (2013). The non-steady state oceanic CO2 signal: Its importance, magnitude and a novel way to detect it. *Biogeosciences*, *10*(4), 2219–2228. https://doi.org/10.5194/bg-10-2219-2013

Menemenlis, D., Campin, J., Heimbach, P., Hill, C. N., Lee, T., Nguyen, A., … J-M. Campin. (2008). ECCO2 : High Resolution Global Ocean and Sea Ice Data Synthesis. *Mercator Ocean Quarterly Newsletter*, *31*(October), 13–21. Retrieved from http://www.mercator-ocean.fr/content/download/691/5904/version/1/file/lettre_31_en.pdf#page=13

Meredith, M. P. (2016). Understanding the structure of changes in the Southern Ocean eddy field. *Geophysical Research Letters*, *43*(11), 5829–5832. https://doi.org/10.1002/2014JC010066.Received

Meredith, M. P., & Hogg, A. M. (2006). Circumpolar response of Southern Ocean eddy activity to a change in the Southern Annular Mode. *Geophysical Research Letters*, *33*(16), 2–5. https://doi.org/10.1029/2006GL026499

Meredith, M. P., Naveira Garabato, A. C., Hogg, A. M., & Farneti, R. (2012). Sensitivity of the overturning circulation in the Southern Ocean to decadal changes in wind forcing. *Journal of Climate*, *25*(1), 99–110. https://doi.org/10.1175/2011JCLI4204.1

Metzl, N., Brunet, C., Jabaud-Jan, A., Poisson, A., & Schauer, B. (2006). Summer and winter air-sea CO2 fluxes in the Southern Ocean. *Deep-Sea Research Part I: Oceanographic Research Papers*, *53*(9), 1548–1563. https://doi.org/10.1016/j.dsr.2006.07.006

Mongwe, N. P., Chang, N., & Monteiro, P. M. S. (2016). The seasonal cycle as a mode to diagnose biases in modelled CO 2 fluxes in the Southern Ocean. *Ocean Modelling*, *106*, 90–103. https://doi.org/10.1016/j.ocemod.2016.09.006

Monteiro, P. M. S., Gregor, L., Lévy, M., Maenner, S., Sabine, C. L., & Swart, S. (2015). Intraseasonal variability linked to sampling alias in air-sea CO2 fluxes in the Southern Ocean. *Geophysical Research Letters*, *42*(20), 8507–8514. https://doi.org/10.1002/2015GL066009

Munro, D. R., Lovenduski, N. S., Takahashi, T. T., Stephens, B. B., Newberger, T., & Sweeney, C. (2015). Recent evidence for a strengthening CO2 sink in the Southern Ocean from carbonate system measurements in the Drake Passage (2002-2015). *Geophysical Research Letters*, *42*(18), 7623–7630. https://doi.org/10.1002/2015GL065194

Nicholson, S. A., Lévy, M., Llort, J., Swart, S., & Monteiro, P. M. S. (2016). Investigation into the impact of storms on sustaining summer primary productivity in the Sub-Antarctic Ocean. *Geophysical Research Letters*, *43*(17), 9192–9199. https://doi.org/10.1002/2016GL069973

Pfeil, B., Olsen, A., Bakker, D. C. E., Hankin, S., Koyuk, H., Kozyr, A., … Yoshikawa-Inoue, H. (2013). A uniform, quality controlled Surface Ocean CO2 Atlas (SOCAT). *Earth System Science Data*, *5*(1), 125–143. https://doi.org/10.5194/essd-5-125-2013

Reynolds, R. W., Smith, T. M., Liu, C., Chelton, D. B., Casey, K. S., & Schlax, M. G. (2007). Daily high-resolution-blended analyses for sea surface temperature. *Journal of Climate*, *20*(22), 5473–5496. https://doi.org/10.1175/2007JCLI1824.1

Rödenbeck, C., Bakker, D. C. E., Gruber, N., Iida, Y., Jacobson, A. R., Jones, S. D., … Zeng, J. (2015). Data-based estimates of the ocean carbon sink variability - First results of the Surface Ocean pCO2 Mapping intercomparison (SOCOM). *Biogeosciences*, *12*(23), 7251–7278. https://doi.org/10.5194/bg-12-7251-2015

Rödenbeck, C., Keeling, R. F., Bakker, D. C. E., Metzl, N., Olsen, A., Sabine, C. L., & Heimann, M. (2013). Global surface-ocean pCO2 and sea-Air CO2 flux variability from an observation-driven ocean mixed-layer scheme. *Ocean Science*, *9*(2), 193–216. https://doi.org/10.5194/os-9-193-2013

Rodgers, K. B., Aumont, O., Mikaloff Fletcher, S. E., Plancherel, Y., Bopp, L., de Boyer Montégut, C., … Wanninkhof, R. H. (2014). Strong sensitivity of Southern Ocean carbon uptake and nutrient cycling to wind stirring. *Biogeosciences*, *11*(15), 4077–4098. https://doi.org/10.5194/bg-11-4077-2014

Sabine, C. L., Hankin, S., Koyuk, H., Bakker, D. C. E., Pfeil, B., Olsen, A., … Yoshikawa-Inoue, H. (2013). Surface Ocean CO2 Atlas (SOCAT) gridded data products. *Earth System Science Data*, *5*(1), 145–153. https://doi.org/10.5194/essd-5-145-2013

Sasse, T. P., McNeil, B. I., & Abramowitz, G. (2013). A novel method for diagnosing seasonal to inter-annual surface ocean carbon dynamics from bottle data using neural networks. *Biogeosciences*, *10*(6), 4319–4340. https://doi.org/10.5194/bg-10-4319-2013

Shetye, S. S., Mohan, R., Patil, S., Jena, B., Chacko, R., George, J. V., … Sudhakar, M. (2015). Oceanic pCO2 in the Indian sector of the Southern Ocean during the austral summer–winter transition phase. *Deep Sea Research Part II: Topical Studies in Oceanography*, *118*, 250–260. https://doi.org/10.1016/j.dsr2.2015.05.017

Swart, N. C., & Fyfe, J. C. (2012). Observed and simulated changes in the Southern Hemisphere surface westerly wind-stress. *Geophysical Research Letters*, *39*(16), 6–11. https://doi.org/10.1029/2012GL052810

Swart, N. C., Fyfe, J. C., Gillett, N., & Marshall, G. J. (2015). Comparing trends in the southern annular mode and surface westerly jet. *Journal of Climate*, *28*(22), 8840–8859. https://doi.org/10.1175/JCLI-D-15-0334.1

Swart, S., Thomalla, S. J., & Monteiro, P. M. S. (2015). The seasonal cycle of mixed layer dynamics and phytoplankton biomass in the Sub-Antarctic Zone: A high-resolution glider experiment. *Journal of Marine Systems*, *147*, 103–115. https://doi.org/10.1016/j.jmarsys.2014.06.002

Tagliabue, A., Bowie, A. R., Philip, W., Buck, K. N., Johnson, K. S., & Saito, M. A. (2017). The integral role of iron in ocean biogeochemistry. *Nature*, *543*(7643), In Press. https://doi.org/10.1038/nature21058

Tagliabue, A., Sallée, J.-B., Bowie, A. R., Lévy, M., Swart, S., & Boyd, P. W. (2014). Surface-water iron supplies in the Southern Ocean sustained by deep winter mixing. *Nature Geoscience*, *7*(March), 314–320. https://doi.org/10.1038/NGEO2101

Takahashi, T. T., Olafsson, J., Goddard, J. G., Chipman, D. W., & Sutherland, S. C. (1993). Seasonal variation of CO 2 and nutrients in the high-latitude surface oceans: A comparative study. *Global Biogeochemical Cycles*, *7*(4), 843–878. https://doi.org/10.1029/93GB02263

Takahashi, T. T., Sutherland, S. C., Sweeney, C., Poisson, A., Metzl, N., Tilbrook, B., … Nojiri, Y. (2002). Global sea-air CO2 flux based on climatological surface ocean pCO2, and seasonal biological and temperature effects. *Deep-Sea Research Part II: Topical Studies in Oceanography*, *49*(9–10), 1601–1622. https://doi.org/10.1016/S0967-0645(02)00003-6

Takahashi, T. T., Sutherland, S. C., Wanninkhof, R. H., Sweeney, C., Feely, R. A., Chipman, D. W., … de Baar, H. J. W. (2009). Climatological mean and decadal change in surface ocean pCO2, and net sea–air CO2 flux over the global oceans. *Deep-Sea Research Part II: Topical Studies in Oceanography*, *56*(8–10), 554–577. https://doi.org/10.1016/j.dsr2.2008.12.009

Thomalla, S. J., Fauchereau, N., Swart, S., & Monteiro, P. M. S. (2011). Regional scale characteristics of the seasonal cycle of chlorophyll in the Southern Ocean. *Biogeosciences*, *8*(10), 2849–2866. https://doi.org/10.5194/bg-8-2849-2011

Wang, S., & Moore, J. K. (2012). Variability of primary production and air-sea CO2 flux in the Southern Ocean. *Global Biogeochemical Cycles*, *26*(1), 1–12. https://doi.org/10.1029/2010GB003981

Wanninkhof, R. H., Asher, W. E., Ho, D. T., Sweeney, C., & McGillis, W. R. (2009). Advances in Quantifying Air-Sea Gas Exchange and Environmental Forcing*. *Annual Review of Marine Science*, *1*(1), 213–244. https://doi.org/10.1146/annurev.marine.010908.163742

Weiss, R. (1974). Carbon dioxide in water and seawater: the solubility of a non-ideal gas. *Marine Chemistry*, *2*(3), 203–215. https://doi.org/10.1016/0304-4203(74)90015-2

Wentz, F. J., Scott, J., Hoffman, R., Leidner, M., Atlas, R., & Ardizzone, J. (2015). Remote Sensing Systems Cross-Calibrated Multi-Platform (CCMP) 6-hourly ocean vector wind analysis product on 0.25 deg grid, Version 2.0. Retrieved March 5, 2017, from www.remss.com/measurements/ccmp

Whitt, D. B., Lévy, M., & Taylor, J. R. (2017). Low-frequency and high-frequency oscillatory winds synergistically enhance nutrient entrainment and phytoplankton at fronts. *Journal of Geophysical Research*, *122*(2), 1016–1041. https://doi.org/10.1002/2016JC012400